https://doi.org/10.5194/egusphere-2026-1914
Preprint. Discussion started: 16 June 2026

Simulating the permafrost thermal regime in the Northwestern Antarctic Peninsula from 1950 to 2100.

Joana Baptista[1], Sebastian Westermann[2], Gonçalo Vieira[1]

[1]Centre of Geographical Studies, Associate Laboratory TERRA, Institute of Geography and Spatial Planning, University of Lisbon, Lisbon, Portugal
[2]Department of Geosciences, University of Oslo, Oslo, Norway

Correspondence to: Joana Baptista (joana–baptista1@edu.ulisboa.pt)

Abstract.

Permafrost underlies most of the Antarctic ice-free areas, being crucial for terrestrial ecosystems, influencing pedogenesis, hydrology, geomorphic dynamics, and the carbon biogeochemical cycle. However, uncertainty in the evolution of permafrost temperature is particularly relevant in the Antarctic Peninsula, a climatic hotspot of the continent where an increase in mean annual air temperature of 3.4 ± 1.2 ºC has been recorded, together with a rise in both the frequency and intensity of warm-weather episodes. The impact on permafrost is difficult to foresee, due to a scarce monitoring network implemented following the International Polar Year in 2007-2008, with limited temporal coverage that constrains trends evaluation. In this study, we simulate past and future permafrost temperature evolution in the Northwestern Antarctic Peninsula using the CryoGrid Community Model at five permafrost observatories from the University of Lisbon's network (PERMANTAR). Simulations forced with ERA5 reanalysis reconstruct ground temperature evolution since 1950, revealing a warming trend at all depths, with mean annual ground surface temperature, temperature at the top of permafrost, and mean annual ground temperature warming at rates between 0.19 and 0.29 ºC dec^{-1}. Four distinct periods are identified since 1950: early sustained warming (1950–1975), highly variable warming and cooling (1975–2000), a short cooling period with increased snowfall (2000–2015), and intense warming after 2015 that accelerates permafrost temperature increases at 20 m depth, resulting in mean annual ground temperatures above -2 ºC. Future projections using the ACCESS-CM2 model under SSP1-2.6, SSP2-4.5, and SSP5-8.5 reveal progressive permafrost degradation and a widespread transition to positive mean annual ground temperatures at 20 m depth during the 21st century, with timing and magnitude strongly influenced by elevation, snow cover duration, and local changes in ocean–atmosphere interactions. In the SSP1-2.6, warming rates ranging from 0.21 ± 0.01 to 0.23 ± 0.01 ºC dec^{-1} are predicted for the sites, resulting in extensive permafrost degradation at low altitude. Under SSP2-4.5, all sites are projected to develop positive mean annual ground temperatures at 20 m between 2049 and 2087, with warming rates ranging from 0.31 ± 0.01 to 0.43 ± 0.01 ºC dec^{-1}, implying increased permafrost degradation and increased susceptibility of coastal terrestrial ecosystems in the Northwestern Antarctic Peninsula to climate-driven change. Under the SSP5-8.5, with warming rates between 0.46 ± 0.01 and 0.62 ± 0.01 ºC dec^{-1}, the degradation of permafrost is predicted to occur more rapidly, with positive mean annual ground temperature values at 20 m reached between 2045 and 2071. The projected warming and associated

https://doi.org/10.5194/egusphere-2026-1914
Preprint. Discussion started: 16 June 2026

permafrost loss will change surface and subsurface hydrology, biochemical fluxes and geomorphological processes, impacting the sensitive terrestrial ecosystems.

1 Introduction

Permafrost underlies most of the Antarctic ice-free areas, which are estimated to represent about 0.5% (45,000-70,000 km²) of its surface, being discontinuous at low altitudes and on the coastal areas of the northern Antarctic Peninsula (Bockheim et al., 2013). Knowledge of permafrost temperature evolution remains scarce due to the limited number, spatial coverage, and short time series of permafrost borehole records, despite efforts during the International Polar Year (2007-2008) to expand the Global Terrestrial Network for Permafrost (GTN-P) (Biskaborn et al., 2019; Bockheim et al., 2013; Hrbáček et al., 2021, 2023; Vieira et al., 2010).

In the Antarctic Peninsula, the lack of data on permafrost temperature evolution is particularly significant, as this region represents a climatic hotspot of the continent. An increase in mean annual air temperature (MAAT) of 3.4 ± 1.2 ºC (from -5.3 ºC in 1946) has been recorded at Esperanza Station (Bockheim et al., 2013; Turner et al., 2020; Vaughan et al., 2003). Although this warming trend was temporarily interrupted by a short cooling period between 1999 and 2015 (Bozkurt et al., 2021; Jones et al., 2019; Oliva et al., 2017; Turner et al., 2020), it has since intensified, with the period being also marked by several warm-weather episodes such as those in February 2020 and 2022 (González-Herrero et al., 2022; Gorodetskaya et al., 2023). These events are associated with the formation of atmospheric rivers, which transport heat and moisture from the mid latitudes to the Southern Ocean (Gorodetskaya et al., 2023; Zou et al., 2023). To improve the knowledge on permafrost temperatures, several studies have applied statistical empirical models across different spatial scales, using air and ground surface temperatures to estimate the temperature at the top of permafrost (TTOP) at a given time. For example, (Obu et al., 2020) used the TTOP model to estimate permafrost temperatures across all Antarctic ice-free areas at a 1 km² resolution. Results for the Antarctic Peninsula show TTOP values ranging from -19 ºC in the mountainous southeastern regions to approximately -1 ºC in the South Shetland Islands. At the local scale, studies mainly focused on the South Shetlands archipelago have also used the TTOP model (Baptista et al., 2025; Ferreira et al., 2017; Hrbáček et al., 2020), emphasizing the importance of incorporating detailed information on ground conditions, lithology, and moisture availability.

Our goal is to implement a modelling approach based on the CryoGrid Community Model (CCM) (Westermann et al., 2023), which integrates site-specific characteristics to estimate ground temperature over defined time periods. Specifically, we simulate recent past conditions using reanalysis data, validate the models against observed permafrost temperature data and project the ground temperature evolution until 2100 using selected Coupled Model Intercomparison Project (CMIP) models in different Recommended Concentration Pathway scenarios (IPCC, 2014; O'Neill et al., 2016).

https://doi.org/10.5194/egusphere-2026-1914
Preprint. Discussion started: 16 June 2026

In Baptista et al. (2025), the performance of the CCM was evaluated for the King Sejong permafrost observatory on Barton Peninsula, King George Island. In this study, five observatories of the PERMANTAR network (http://permantar.weebly.com) distributed along the Northwestern Antarctic Peninsula are used for CCM application.

2 Study area

2.1 Western Antarctic Peninsula

The Antarctic Peninsula, located between 60º S and 75º S, is dominated by a long mountain range formed as a result of volcanic activity that occurred between 183 and 4 million years ago (Fox, 2019). Most of the surface is covered by glaciers, with ice-free areas remaining on mountain peaks, steep rock faces and peninsulas at low altitude.

The coastline is bounded by numerous islands and archipelagos that form a network of straits and channels, such as the Palmer Archipelago off the northwestern coast, separated from the peninsula by the Gerlache Strait, and the South Shetland Islands to the north of the peninsula, separated by the Bransfield Strait. On the eastern coast, the peninsula is bordered by the Larsen Ice Shelf, which extends between approximately 64º S and 70º S.

Acting as a natural barrier to atmospheric circulation, the Antarctic Peninsula is divided in two distinct climatic regions: a western region, characterized by a polar maritime climate influenced by the Bellingshausen Sea and exposed to continuous passage of moist frontal systems from the Pacific and the Drake Passage, and an eastern region, on the Weddell Sea side, sheltered by the peninsula, with a cold continental climate (Thomas e Tetzner 2019). In the western region, a general warming trend has been observed since the 1950s. Studies by Bozkurt et al. (2022), Gorodetskaya et al. (2023) and Zou et al. (2023) revealed an increase in the frequency and intensity of warm episodes associated with the formation of atmospheric rivers. These events result in intense rainfall combined with warm temperatures which impact the cryosphere by forcing positive feedback that enhance and accelerate the warming trend, leading to the melting of glaciers and ice shelves, and increase in the active layer thickness (Thomas e Tetzner 2019).

2.2 The PERMANTAR Northwestern Antarctic Peninsula Permafrost Observatories Network

The PERMANTAR monitoring sites analyzed in this paper are installed in four ice-free areas located along a gradient from 62º S to 64º S in the Northwestern Antarctic Peninsula (Fig. 1 and Appendix A, Fig. A1): Barton Peninsula, Hurd Peninsula, Cierva Point and Amsler Island.

https://doi.org/10.5194/egusphere-2026-1914
Preprint. Discussion started: 16 June 2026

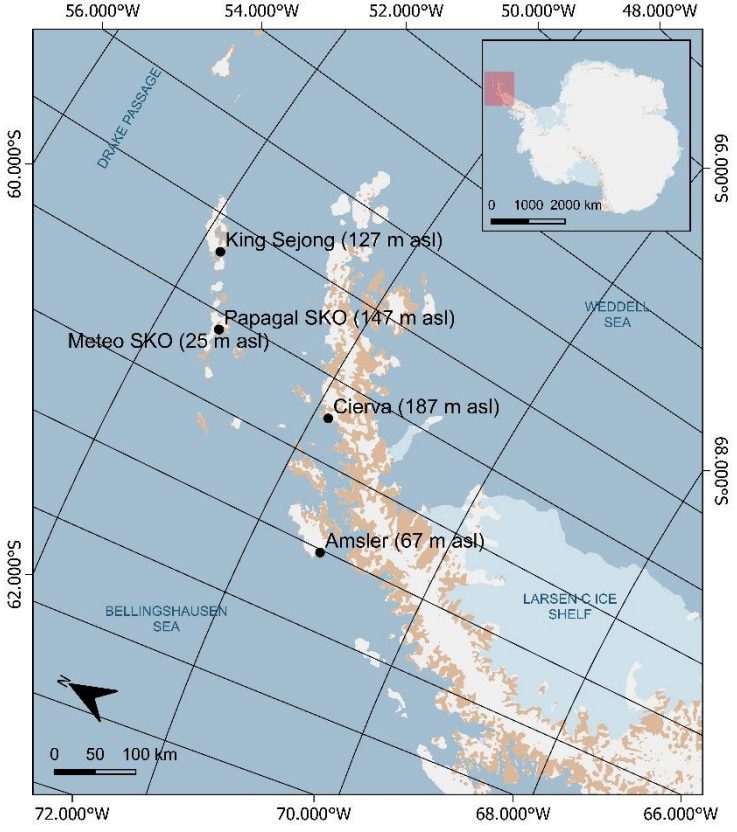

Figure 1: Location in the Northwestern Antarctic Peninsula of the PERMANTAR observatories analyzed. Basemap from Quantartica dataset (Matsuoka et al., 2018).

2.2.1 Barton Peninsula, King George Island

The northernmost observatory is installed on Barton Peninsula in King George Island (South Shetlands Archipelago). With an ice-free area of 10 km^2, this peninsula was exposed between 15 and 3.7 ka BP due to the retreat of the Collins Glacier (Oliva et al., 2019). The relief is dominated by a west-east ridge (290 m asl) associated with a plutonic intrusion. At lower elevation, two plateaus are present, at 170 and 130 m asl, formed by volcanic strata dominated by andesitic lava flows with frequent dykes (Birkenmajer, 1989; Hwang et al., 2011; Kim et al., 2002). Cliffs characterize the western and southern coasts, while on the northern coast, a moderate and stepped slope connects the plateaus to a series of raised beaches. The climate is polar maritime with a MAAT of -2.3 ºC, recorded at Bellingshausen station (16 m asl) from 1969 to 2020, and annual precipitation of 534 mm, measured on King Sejong Station at 11 m asl from 2005 to 2019 (Baptista et al., 2024).

https://doi.org/10.5194/egusphere-2026-1914
Preprint. Discussion started: 16 June 2026

2.2.2 Hurd Peninsula, Livingston Island

The Papagal and SKO station observatories are installed in Hurd Peninsula in Livingston Island (South Shetland Archipelago). With an ice-free area of about 20 km^2, the highest areas of Hurd Peninsula were deglaciated at 20 ka with most high interfluves becoming ice-free around 14-16 ka and the lower valleys around 7.5 ka. The mid-Holocene showed Neoglacial advances at ca. 4.5 ka, with deglaciation following subsequently (Oliva et al., 2024). The peninsula features rock outcrops belonging to the shales and quartzites of the Miers Bluff Formation and small areas of granites and dykes swarms, as well as till and moraine ridges along the deglaciated valleys, and widespread angular debris mantling slopes and interfluves (Fernández-Fernández et al., 2021; Ferreira et al., 2017; Kraus et al., 2008; Lopez-Martinez et al., 1992). The highest elevation is Moores Peak with 390 m asl. The climate is polar maritime, with a MAAT of -2 ºC and annual precipitation between 500 to 800 mm at the sea level (Fernández-Fernández et al., 2021).

2.2.3 Cierva Point, Antarctic Peninsula

On the Danco Coast of the Western Antarctic Peninsula, Cierva Point is a small ice-free area of approximately 2 km². Sheltered from the open sea by Brabant Island to the west, the area has rugged relief, with the highest elevation located at 340 m asl. Granodiorite outcrops are dominant on the northernmost lowlands, featuring polished surfaces and striations that indicate recent exposure (Wilhelm et al., 2016). At lower elevations, moraine accumulations are found, composed of granite debris. On the middle of the ice-free area orthoclase feldspar granites are present. The eastern and southern areas are dominated by basalts. Closer to the sea, marine terraces are found, containing unconsolidated materials derived from weathered bedrock (Wilhelm et al., 2016). The climate is polar maritime, with a MAAT of -3.2 ºC, recorded at 50 m asl, and annual precipitation ranging from 400 to 1100 mm (Wilhelm et al., 2016).

2.2.4 Amsler Island, Palmer Archipelago

The southernmost monitoring site, Amsler Island, is situated southeast of Anvers Island close to Palmer station. The relief is defined by an east-west glacial valley that divides the island (Wilhelm and Bockheim, 2017). The valley floor is filled with outwash sands overlying lacustrine sediments. On the southern boundary of the valley, solifluction lobes are found associated with outwash sediments. On the northern boundary, moraines are present comprising unsorted materials from silts to boulders (> 3 m diameter). The area that surrounds the central valley is characterized by a bare igneous bedrock with frost shattered fragments (Wilhelm and Bockheim, 2016). The highest point is located on the north sector at 68 m asl, in an interfluve surrounded by steep bedrock slopes. Under a polar maritime climate, the MAAT is of -1.8 ºC at 8 m asl, with annual precipitation ranging from 714 to 1410 mm (Wilhelm and Bockheim, 2017).

https://doi.org/10.5194/egusphere-2026-1914
Preprint. Discussion started: 16 June 2026

3 Materials and methods

3.1 PERMANTAR monitoring sites

PERMANTAR is the University of Lisbon's network of permafrost observatories in the Northwestern Antarctic Peninsula. As a contributor to the Global Terrestrial Network for Permafrost (GTN-P), the network includes nine monitoring sites. Of these, five were selected for the analysis of the recent and future evolution of permafrost temperatures: The King Sejong observatory, located on King George Island, the Papagal and SKO Station observatories, located on Livingston Island, the Cierva observatory, in Cierva Point, and finally, the Amsler observatory on Amsler Island (Fig. 1 and Table 1). These observatories were selected because the boreholes are installed in bedrock and have larger depth, allowing for better representation of permafrost temperatures, and to reduce site heterogeneity and modelling complexity. Detailed descriptions of the monitoring sites are provided in Appendix A.

From the five observatories, in 2022 permafrost was present only at King Sejong (-1.3 ºC at 13 m depth) with an active layer thickness (ALT) of 3 m, and at Cierva (-1.2 ºC at 15 m depth) with an ALT of 5 m. On the remaining observatories, at the maximum borehole depth (4 to 9 m), permafrost was not reached, but permafrost is known to occur just below the borehole in Papagal, as in cold years the base of the active layer is within the borehole.

Table 1: Characteristics of the PERMANTAR observatories analyzed in this study.

Observatory	Coordinates	Elevation (m)	Installation	Instruments	Measurement height/depth (m)
King Sejong	62.228883 ºS 58.770317 ºW	127	2019	Borehole Surface temperature Air temperature	13 0.02 1.5
Papagal	62.648389 ºS 60.363694 ºW	147	2008	Borehole Surface temperature Air temperature	4 0.02 1.5
SKO Station	62.641420 ºS 60.363970 ºW	25	2009	Borehole Surface temperature Air temperature	8 0.02 1.5
Cierva	64.161950 ºS, 60.950933 ºW	187	2012	Borehole Surface temperature Air temperature	15 0.02 1.5
Amsler	64.761533 ºS 64.074250 ºW	67	2012	Borehole Surface temperature Air temperature	9 0.02 1.5

3.2 CryoGrid community model

3.2.1 Model description

The CryoGrid community model is a flexible toolbox developed to simulate the ground thermal regime including the water and ice balance of permafrost and glaciers (Westermann et al. 2023). It enables the combination of different modules (referred

https://doi.org/10.5194/egusphere-2026-1914
Preprint. Discussion started: 16 June 2026

to as "classes" in the following) representing snow conditions, vegetation cover, and subsurface materials under a variety of scenarios. In its current version, CCM is based on an object-oriented approach implemented in MATLAB, which allows for the creation of a hierarchical structure where variables and functions are organized through the stacking of different classes. These classes are associated with a vertical domain and can represent ground columns with or without water balance, water bodies, and glaciers (Westermann et al., 2023).

3.2.2 Model calibration

The model calibration has two phases. In the first, subsurface parameters are evaluated, while in the second the surface energy model is validated, following the approach adopted in Baptista et al. (2025).

For the evaluation of the subsurface parameters, a class representing a ground column with temperature boundary condition at the surface (GROUND_freeW_ubT, Westermann et al., 2023) was selected, for which water phase change occurs at 0 ºC and the sum of water and ice contents remain constant (Baptista et al., 2025). Measured ground surface temperature from the PERMANTAR monitoring sites was used as upper boundary input while the geothermal heat flux of 50 mWm^{-2} was applied as the lower boundary. With the structure set, 1D simulations were run with different configurations of mineral, water/ice and organic relative volumetric content for each of the five boreholes. Additionally, the thermal conductivity was updated based on the thermophysical analysis performed on the rock cores. In this analysis, the cores were sliced, and the clean surface was used to measure the conductivity with the ISOMET 2104 instrument using a probe. From each simulation, estimated daily average ground temperatures at 4 depths (0.4, 1.2, 3.0, and maximum depth of borehole) were extracted to be compared with the observational records. The metrics used for the assessment of model performance were bias, correlation coefficient (r), mean absolute error (MAE) and root mean square error (RMSE).

In the evaluation of the model results, the best configuration of relative volumetric content was used in a ground class (GROUND_freeW_seb_snow) in which the phase change of water again occurs at 0 ºC and the water and ice contents remain constant. However, the surface energy balance is applied to simulate energy exchange processes between the atmosphere and the model's first grid cell (Baptista et al. 2025; Westermann et al. 2023). To use the surface energy balance component of the model, the simulations are forced with bias-corrected ERA5 reanalysis (see Sect. 3.3.1) near-surface variables i.e. incoming short- and longwave radiation (S_{in} and L_{in}) [Wm^{-2}], solid and liquid precipitation (P_s and P_l) [mm d^{-1}], air pressure (p) [Pa], air temperature ($Tair$) [ºC], wind speed (U) [m s^{-1}], and specific humidity ($qair$) [kg water vapour kg air^{-1}] (Westermann et al., 2023). The energy flux into the uppermost grid cell is calculated through Eq. (1), where S_{out} and L_{out} are the outgoing short- and longwave radiation and Q_h and Q_e the sensible and latent heat flux.

$$F_{ub}(t) = S_{in}(t) - S_{out}(t) + L_{in}(t) - L_{out}(t) - Q_h(t) - Q_e(t) \quad (1)$$

The heat conduction based on Fourier's law is the main mode of heat transport in the subsurface.

https://doi.org/10.5194/egusphere-2026-1914
Preprint. Discussion started: 16 June 2026

When the ground is snow-covered, the ground class is stacked below a snow class (SNOW_crocus_bucketW_seb) that represents the seasonal snow microphysics scheme following the Crocus model (Vionnet et al., 2012; Zweigel et al., 2021). The snow model represents transient snow density changes due to compaction and wind drift, as well as meltwater infiltration and refreezing. Due to the micro topography at each monitoring site and to the spatial resolution of ERA5 variables, an over- or underestimation of snow depth can be produced by the model. Previous studies reported that ERA5 often overestimates snow cover in coastal Antarctic areas (Boike et al. 2019; Gisnås et al. 2014; Obu et al. 2020), due to unrepresented topography and ice-free vs glacier surfaces and wind redistribution effects. Therefore, ERA5-derived snowfall P_s was corrected for each site using a snow multiplication factor which allows a phenomenologically increase or reduction of the simulated snow depth based on the intensity of the insulating effect and duration of the snow cover (Zweigel et al., 2021). As for the first phase, the validation of the surface energy model was performed through the comparison between the estimated and measured ground temperatures at 4 depths and the analysis of the four statistical measures (bias, *r*, MAE and RMSE).

3.3 Model forcing

3.3.1 ERA5

ERA5 is based on the Integrated Forecasting System (IFS) Cy41r2 and combines model data with observations using a data assimilation approach allowing a detailed record of the global atmosphere, land surface and ocean waves from 1950 onwards, hourly, with a horizontal resolution of 31 km (Hersbach et al., 2020).

In this study, the simulation of the past evolution of permafrost temperature with the CCM, uses surface level data from ERA5 interpolated to the location of each monitoring site (Copernicus Climate Change Service, 2023). The following variables were obtained from the Copernicus Climate Data Store: (a) surface solar radiation downwards [J m^{-2}], (b) surface thermal radiation downwards [J m^{-2}], (c) total precipitation [m], (d) 10 m u component of wind [m s^{-1}], (e) 10 m v component of wind [m s^{-1}], (f) surface pressure [Pa], and (g) 2 m dew point temperature [K].

Concerning the performance, Zhu et al. (2021) while assessing the ERA5 reanalysis for Antarctic near-surface air temperature against in-situ measurements from 41 weather stations across Antarctica, identified regional and seasonal biases, including a warm bias inland and difficulties in capturing local variability in complex terrain. However, the results were better when compared to the ERA-Interim. In same context Jones and Lister (2015) emphasize that the extreme and remote conditions of Antarctica pose significant challenges for data assimilation, contributing to potential biases in surface temperature and precipitation estimates.

For the Antarctic Peninsula, Tetzner et al. (2019) identified a seasonal cold bias on the 2 m air temperature and an underestimation of wind speed in coastal regions despite a good representation of the wind regimes. At Barton Peninsula, Baptista et al. (2025) compared ERA5-derived air temperature and in situ measurements, revealing a cold bias during the summer season. Here, the ERA5-derived air temperature at four of the observatories (King Sejong, Papagal, Cierva and

https://doi.org/10.5194/egusphere-2026-1914
Preprint. Discussion started: 16 June 2026

Amsler) was corrected following Westermann et al. (2016), in which a linear regression is used to correct the average bias and trend of model forcing (Table 2). At the low elevation SKO Station borehole, quantile mapping provided a better representation of the thermal amplitude and a reduction of the strong warm bias being used instead (Table 2). Comparison between ERA5-derived air temperature, ERA5-derived air temperature bias corrected and in situ measurements at the PERMANTAR observatories are provided in Appendix B.

Table 2: Analysis of ERA5 derived air temperature and bias corrected air temperature on the PERMANTAR observatories

Observatory	ERA5 derived air temperature				ERA5 derived air temperature bias corrected			
	r	MAE	RMSE	p-value	r	MAE	RMSE	p-value
King Sejong	0.97	0.87	1.20	< 0.01	0.97	0.62	0.86	< 0.01
Papagal	0.95	0.92	1.21	< 0.01	0.98	0.58	0.79	< 0.01
SKO Station	0.89	1.16	1.58	< 0.01	0.90	1.04	1.49	< 0.01
Cierva	0.89	1.58	2.05	< 0.01	0.92	1.14	1.50	< 0.01
Amsler	0.87	1.47	2.05	< 0.01	0.93	1.11	1.49	< 0.01

3.3.2 CMIP6 scenarios and models

The CMIP coordinates the design and distribution of global climate model simulations of the past, current, and future climate, derived from natural, unforced variability or in response to changes in radiative forcings (Eyring et al., 2016; IPCC, 2013). CMIP simulations are based on the different scenarios defined by the Intergovernmental Panel on Climate Change (IPCC), which describe possible future developments of anthropogenic drivers according to the socioeconomic development (O'Neill et al., 2016). These scenarios are referred as future Shared Socioeconomic Pathways (SSPs) and are associated to the former Representative Concentration Pathways (RCPs) (IPCC, 2014; O'Neill et al., 2016). The RCPs are used to represent 4 pathways of GHG emissions and atmospheric concentrations driven by population size, economic activity, lifestyle, energy used, land use patterns, technology and climate policy (IPCC, 2014).

In this study, the simulation of future permafrost temperature with the CCM, uses three scenarios from the CMIP6 (IPCC, 2014; O'Neill et al., 2016):

- *SSP1-2.6:* represents an optimistic trend of human development, with substantial investments in education and health, rapid economic growth and functioning institutions, associated with an increasing shift towards sustainable practices in which global warming will stay below 2ºC.

https://doi.org/10.5194/egusphere-2026-1914
Preprint. Discussion started: 16 June 2026

- *SSP2-4.5:* simulates a central pathway in which the trend continues the historical pattern without substantial deviation, and global warming varying from 2 to 3ºC.
- *SSP5-8.5:* predicts a trend of human development with substantial investments in education and health, rapid economic growth, and functioning institutions, but based on intensive energy consumption and a fossil-based economy, in which global warming will range from 3 to 5 ºC.

The INM-CM4-8, the IPSL-CM6A and the ACCESS-CM2 models from CMIP6 were evaluated, as they provide adequate data to force the CCM. The INM-CM4-8 incorporates several modules as subcomponents: atmospheric (INM-AM4-8, 21 levels), aerosol (INM-AER1), land (INM-LND1), ocean (INM-OM5), and sea ice (INM-ICE1), operating at nominal resolution of 100 km (Volodin et al., 2019). The IPSL-CM6A integrates atmospheric (LMDZ), oceanic (NEMO-OPA), land surface (ORCHIDEE), and sea ice components (NEMO-LIM3) (Bonnet et al., 2021). It also incorporates a representation of the carbon cycle and interactive stratospheric and tropospheric chemistry with aerosols. The model operates at nominal resolutions of 250 km for the atmosphere and land surface and 100 km for ocean and sea ice components. The ACCESS-CM2 includes components models for the atmosphere (MetUM-HadGEM3-GA7.1, 85 vertical levels), aerosols and atmospheric chemistry (GLOMAP and UKCA), land (CABLE2.5), ocean (GFDL-MOM5, 50 vertical levels) and sea-ice (CICE5.1.2, 50 vertical levels) (Bi et al., 2020). It operates at nominal resolutions of 250 km for the atmosphere, aerosol and land surface and 100 km for ocean and sea ice components.

Following the evaluation, the ACCESS-CM2 model was selected to simulate the future evolution of permafrost temperatures having a correlation to ERA5 of 0.70 ($p<0.001$), a MAE of 1.16 ºC and RMSE of 1.33ºC. Detailed information on the three models, as well as the results of their evaluation, are provided in Appendix C.

Data was downloaded from the Climate Data Store (Copernicus Climate Change Service, 2021) for the historical, the SSP1-2.6, the SSP2-4.5 and the SSP5-8.5 scenarios. The variables for forcing the simulation were: (a) near-surface air temperature [K], (b) near-surface specific humidity [dimensionless], (c) near-surface wind speed [m s^{-1}], (d) precipitation [kg m^{-2} s^{-1}], (e) surface air pressure [Pa], (f) surface downwelling longwave radiation [W m^{-2}], (g) surface downwelling shortwave radiation [W m^{-2}], (h) Top Of Atmosphere (TOA) incident shortwave radiation [W m^{-2}].

3.4 Simulation of the past evolution of permafrost temperatures

The simulation of the past evolution, forced with ERA5 reanalysis aimed to reconstruct permafrost temperatures from 1950 to 2020 in the selected PERMANTAR monitoring sites. Since the initial ground temperature profile is unknown, the simulation was run with an accelerated spin-up using the first 10 years of the ERA5 reanalysis (1940-1949) looped 10 times. This allowed for the definition of the temperature profile at the beginning of the modeling period, using the parameters and stratigraphy defined for each monitoring site (Westermann et al., 2023). Then, the simulation advances for the full ERA5 time series.

https://doi.org/10.5194/egusphere-2026-1914
Preprint. Discussion started: 16 June 2026

The simulation's output produces an estimation of ground temperatures for a profile of 20 m depth with a vertical resolution ranging from 0.05 to 0.5 m, below 5 m depth. These estimations were used to calculate the mean annual ground surface temperature (MAGST), mean annual ground temperature (MAGT) and temperature at the top of permafrost (TTOP).

3.5 Simulation of the future evolution of permafrost temperatures

While the CMIP6 model output in principle provides the near-surface variables required to force the CCM, the coarse grid and simplified representations of key processes generally produce biases in permafrost simulations (Westermann et al., 2016). In most cases, this leads to a misrepresentation of present-day permafrost conditions in the CCM output, which compromises any future projections of ground thermal regime, in particular when permafrost thaws and ground temperatures increase above the melting point of ground ice. For this reason, we synthesized a model forcing time series from the site-corrected ERA5 records (referred to as ERA5 in the following) and monthly CMIP6 output, spanning the entire CMIP6 period from 1850 to 2100. For each model forcing variable, we calculated a statistical relationship between the average CMIP6 output and the average of the ERA5 data for each month of the year for an overlap period from 1940 to 2020, which is then used to bias-correct the synthesized 1850 to 2100 time series. We first calculated the mean M_i and standard deviation μ_i of the entire overlap period for each month of the year i (from 1 to 12) for both the ERA5 and CMIP6 data. We then produced a bias-corrected time series of monthly CMIP6 averages by adjusting both the mean and the standard deviation as:

$$V_{i,y}^{CMIP,corrected} = V_{i,y}^{CMIP} + M_i^{ERA5} - M_i^{CMIP} + {\mu_i^{ERA5}}/{\mu_i^{CMIP}} \left(V_{i,y}^{CMIP} - m_i^{CMIP}\right), \quad (2)$$

in which $V_{i,y}$ denotes the average value of a model forcing variable in a particular month *i* and a particular year *y* between 1850 and 2100. m_i^{CMIP} is equal to M_i^{CMIP} during the overlap period, while it is set to the running mean of 10-year periods for the remainder of the time series, so that short-term fluctuations can be separated from multi-annual trends (which are accounted for by the first three terms on the right-hand side). With this procedure, we ensure that the corrected CMIP6 data features the same monthly mean and standard deviation as the ERA5 data for the overlap period. As "carrier" for the synthesized time series, we randomly sample individual months from the ERA5 time series for each month of the year, which provides somewhat realistic weather conditions on below-monthly timescale. Finally, the carrier data are again corrected on the basis of monthly averages with the corrected CMIP6 time series by adding the offset.

$$\Delta V_{i,y} = V_{i,y}^{CMIP,corrected} - V_{i,y}^{carrier}, \quad (3)$$

in which $V_{i,y}$ refers to the monthly average of the corrected CMIP6 and the carrier data, respectively. This procedure of using absolute deviations is applied for near-surface air temperature, relative humidity (which is calculated from the specific

https://doi.org/10.5194/egusphere-2026-1914
Preprint. Discussion started: 16 June 2026

humidity for both time series), surface air pressure and downwelling longwave radiation, while a corresponding scheme with relative corrections is applied for downwelling shortwave radiation, wind speed and precipitation. Here, we first calculate the fractions $v_{i,y}^{ERA5,CMIP} = V_{i,y}^{ERA5,CMIP} / M_i^{ERA5,CMIP}$ for both the monthly ERA5 and CMIP6 data to which the absolute bias correction procedure is applied. The final time series is then again obtained by multiplying with M_i^{ERA5}, i.e. the monthly average of the ERA5 data in the overlap period.

The simulation of the future evolution of permafrost temperature is conducted from 1850 to 2100 for three future scenarios. For these simulations we use the actual ERA5 data, which represents the climatic and weather conditions and for which the model validation was performed between 1940 and 2022, while the statistically correct synthesized time series is employed for other periods.

The model simulation starts with the historical experiment, when the initial ground temperature profile is calculated through an accelerated spin-up using the first 10 years of the synthesized time series looped 10 times (1850-1860), followed simulations from 1850 to 1939. From 1940 to 2022, the simulation advances using the ERA5 series, when it switches to the synthesized CMIP6 series according to each climate change scenario. The simulation's output produces an estimation of ground temperatures for a profile of 20 m depth, used to calculate the MAGST and MAGT which allowed the projection until 2100 according to three scenarios. In the figures, the x-axis spans the period 2000-2100.

4 Results

4.1 Sensitivity analysis to subsurface parameterization and validation of the surface energy model

In the sensitivity analysis of subsurface parameters, the simulations at the five observatories forced with measured ground surface temperature enabled the identification of optimal combinations of mineral, organic matter, water, and ice contents that improved the model performance. These optimized configurations were then applied in simulations forced with ERA5 reanalysis data, allowing for the validation of the surface energy balance model.

As all observatories have boreholes in bedrock, the sensitivity analysis consistently returned high mineral content values (99-100%) (Table 3). Accurate simulation of heat propagation at depth depended on adjusting the rock thermal conductivity. These adjustments, based on values measured from rock cores extracted from the boreholes, were crucial for reproducing the thermal conditions at the sites, as evidenced by the comparison between measured and estimated ground temperature (Appendix D and Fig. D1). Average bias ranged from -0.8 to 0.3 ºC (Table 3). Correlation coefficients exceeded 0.61, with stronger correlations nearer to the surface (Table 3). MAEs were consistently below 1.2 ºC and RMSEs ranged from 0.10 to 1.65 ºC.

In three of the observatories, simulations that included 1% water and ice content were used to represent slightly fractured bedrock (Table 3). This inclusion in the ground stratigraphy settings improved the model's ability to represent the zero-curtain effect, indicating the influence of latent heat, observed during the transition from freezing to thawing seasons, especially at 3

https://doi.org/10.5194/egusphere-2026-1914
Preprint. Discussion started: 16 June 2026

m depth (Appendix D and Fig. D1). The latent heat effects in the near-surface layer is a common feature in maritime Antarctic environments (Almeida et al. 2017; Guglielmin et al. 2014).

Snowfall multiplier values were determined by comparing measured and estimated ground temperatures at a depth of 0.4 m (Fig. 2 and Appendix D and Fig. D1). Initial simulations using ERA5 snowfall data resulted in an overestimation of snow accumulation resulting in excess insulation. Consequently, snow multiplication fractions were reduced across all observatories, ranging from 30% to 50% of the original ERA5 snowfall input.

A snowfall multiplier of 50% was used for the SKO Station, Papagal, Cierva and Amsler observatories, while King Sejong observatory required a snowfall multiplier of 30%. For these four sites, the correlation between measured and simulated ground temperatures at 0.4 m depth ranged from 0.86 to 0.96, with bias varying from -0.7 to 0.1ºC, MAEs between 0.92 and 1.16 ºC, and RMSE values from 1.11 to 1.65 ºC (Table 3).

Table 3: Sensitivity analysis to the surface and subsurface parameters

Observatory	Parameters				Depths (m)	Bias	r	MAE	RMSE	p-value
	Mineral content	Water / ice content	Conductivity W mK^{-1}	Snowfall multiplier						
King Sejong	0.99	0.01	2.10	0.3	0.4	0.3	0.96	0.68	0.92	< 0.01
					1.2	0.1	0.98	0.48	0.59	< 0.01
					3.0	0.2	0.98	0.31	0.37	< 0.01
					13.0	0.1	0.61	0.08	0.16	< 0.01
Papagal	0.99	0.01	2.12	0.5	0.4	-0.7	0.94	0.92	1.11	< 0.01
					1.2	-0.3	0.95	0.73	0.92	< 0.01
					3.0	-0.7	0.91	0.71	0.75	< 0.01
					4.0	-0.6	0.87	0.70	0.70	< 0.01
SKO Station	0.99	0.01	2.12	0.5	0.4	-0.6	0.96	0.98	1.21	< 0.01
					1.2	-0.6	0.95	0.98	1.24	< 0.01
					3.0	-0.6	0.85	0.74	0.96	< 0.01
					8.0	-0.8	0.74	0.62	0.63	< 0.01
Cierva	1.00	0.00	2.70	0.5	0.4	0.1	0.86	1.16	1.65	< 0.01
					1.2	-0.1	0.90	0.82	1.08	< 0.01
					3.0	-0.1	0.93	0.46	0.56	< 0.01
					15.0	-0.1	0.80	0.09	0.10	< 0.01
Amsler	1.00	0.00	3.00	0.5	0.4	-0.3	0.94	1.01	1.33	< 0.01
					1.2	-0.7	0.96	0.86	1.12	< 0.01
					3.0	-0.7	0.97	0.68	0.79	< 0.01
					9.0	-0.4	0.87	0.44	0.48	< 0.01

Seasonally, the estimated temperatures show good agreement with the observations at the five observatories, despite a generally narrower range and less severe extremes (Fig. 2).

At 0.4 m depth, the sensitivity to seasonal changes is reflected in the temperature ranges, which become wider during September, October, and November (SON), reaching a maximum of 16 ºC at King Sejong, followed by SKO Station (11 ºC) and Amsler (11 ºC) (Fig. 2). Papagal and Cierva display slightly narrower temperature ranges, between 5 and 6 ºC. This period

https://doi.org/10.5194/egusphere-2026-1914
Preprint. Discussion started: 16 June 2026

corresponds to the transition from winter to summer, when snow cover begins to melt. Due to the rapid melting of snow cover, these three observatories exhibit more pronounced extremes compared to those where snow persists longer, having an insulation effect which limits the cooling and delays the warming.

During December, January, and February (DJF), temperature ranges in the estimates are generally narrower, with less extreme values (Fig. 2). However, the Papagal and Cierva observatories show distinct characteristics. At Papagal, the estimated temperature range is wider (9 ºC), spanning from -3.2 to 5.7 ºC, though both limits are lower than those from the observations (-1.0 ºC and 7.1 ºC), indicating colder temperatures when compared to the observations. At Cierva, the estimated range (7 ºC) is narrower than that from observations (10 ºC). However, the median from the estimates (2.8 ºC) is higher than the median from the observations (1.2 ºC). Differences in the distribution are also evident in the quantiles, as estimated temperatures between the first and third quantiles align with the second and third quantiles from the observations, indicating generally warmer modeled conditions (Fig. 2). From March to May (MAM), when temperatures oscillate around 0 ºC, the ranges between minima and maxima values in both estimates and observations remain similar, varying from 9 to 11 ºC, with nearly coincident quantiles.

From June to August (JJA), when temperatures are negative, the maximum thermal range varies among the five observatories from 5 to 10 ºC (Fig. 2). The difference is smaller at Papagal and Cierva, where the estimated range (5 ºC) is slightly narrower than the observed ranges (6 and 7 ºC). These observatories, located at 147 and 187 m asl and characterized by a 50 % snow factor, record higher minimum temperatures (-8 to -7 ºC), suggesting snow accumulation with a significant insulating effect during winter. At the remaining observatories, the temperature range is broader (7 to 10 ºC), particularly in the observations. In those cases, minimum temperatures drop below -8 ºC.

When analyzing the seasonal regime at 3 m depth, SKO Station, Cierva, and Amsler display a similar pattern, with observations generally showing higher values and wider ranges between minimum and maximum temperatures compared to the estimates (Fig. 2). Temperatures fluctuate between positive (5 ºC) and negative (-5 ºC) values during DJF and MAM, and remain negative (0 to -5 ºC) during JJA and SON.

At King Sejong, during DJF and MAM, temperatures vary around 0 ºC, with a difference between minimum and maximum values below 1 ºC, suggesting proximity to the top of the permafrost. From JJA to SON, the temperature range increases (1 to 4 ºC), with the estimates showing higher values than the observations.

At the maximum borehole depth at King Sejong, SKO Station, Cierva, and Amsler, temperature variations are minimal (< 1 ºC) (Fig. 2). However, observed temperatures are slightly higher than those estimated by the simulation.

https://doi.org/10.5194/egusphere-2026-1914
Preprint. Discussion started: 16 June 2026

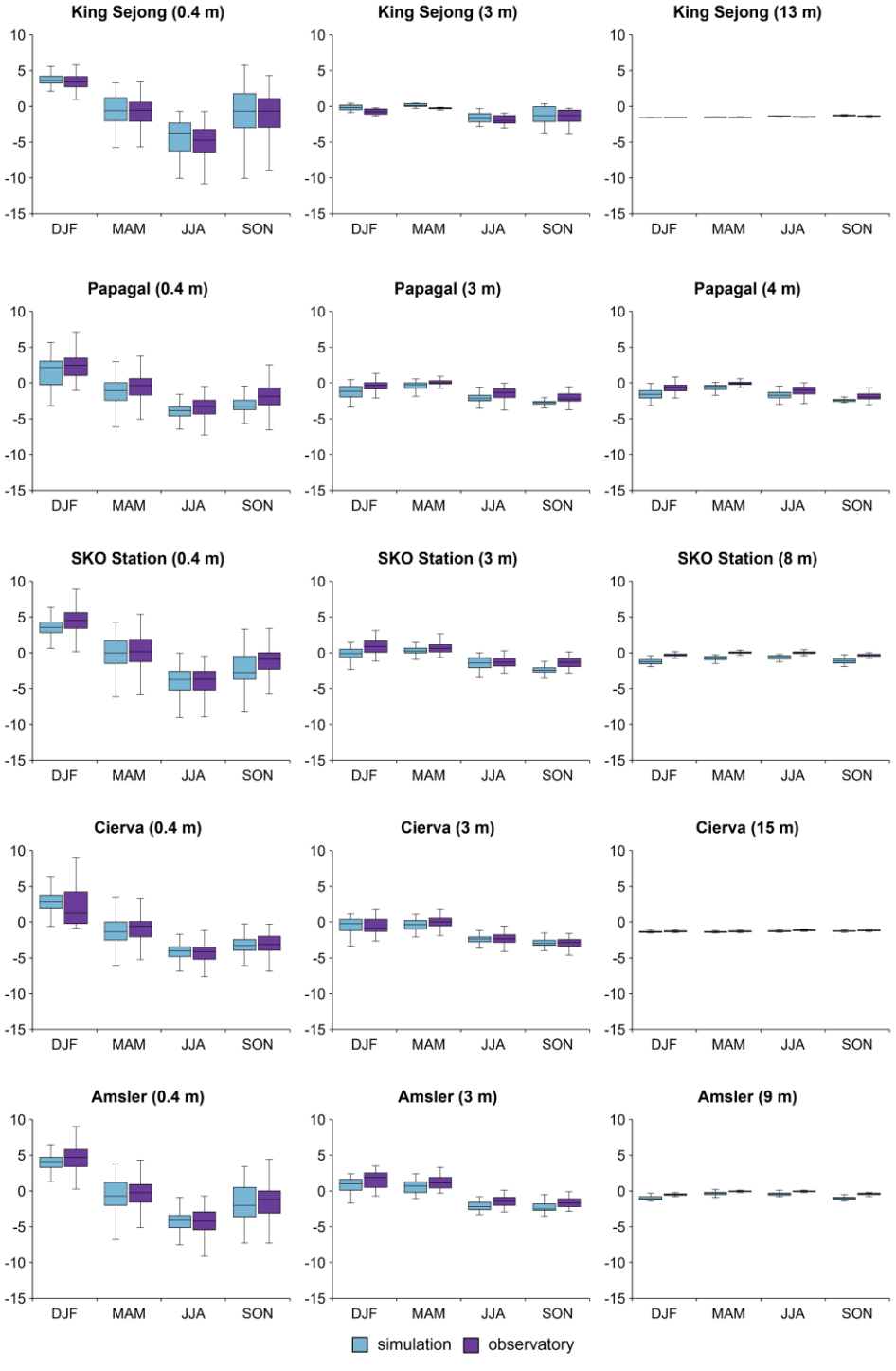

Figure 2: Seasonal variation (DJF, MAM, JJA and SON) of simulated vs observed ground temperatures on the PERMANTAR observatories.

https://doi.org/10.5194/egusphere-2026-1914
Preprint. Discussion started: 16 June 2026

4.2 Past evolution of permafrost temperature (1950 - 2020)

The simulation of ground temperatures since 1950 enabled the reconstruction of past permafrost temperature evolution, revealing a general warming trend in ground temperatures at all depths (Fig. 3 and Table 4). At surface, the highest warming rate was obtained for the southernmost observatory, located at 67 m asl on Amsler Island (0.27 ± 0.04 ºC dec⁻¹), followed by the northernmost observatory, located at 127 m asl on Barton Peninsula (0.25 ± 0.03 ºC dec⁻¹). The remaining observatories exhibited warming rates ranging from 0.19 to 0.22 ºC dec⁻¹ (Table 4).

TTOP values reflect the warming trends observed in MAGST, showing a similar spatial pattern (Fig. 3 and Table 4). The highest TTOP warming rate was again recorded at the Amsler observatory (0.29 ± 0.02 ºC dec⁻¹). This was followed by King Sejong observatory (0.26 ± 0.02 ºC dec⁻¹). At Hurd Peninsula the SKO Station observatory at 25 m asl showed a higher warming rate (0.23 ± 0.02 ºC dec⁻¹) than the nearby Papagal observatory at 147 m asl (0.22 ± 0.02 ºC dec⁻¹). TTOP values at SKO Station were higher overall, ranging from -3 to -0.2 ºC, whereas Papagal exhibited TTOP values between -4 and -1 ºC. At Cierva observatory, where the warming rate of MAAT was the lowest, TTOP values ranged from -4 to -1 ºC and had the lowest warming rate among the sites (0.21 ± 0.02 ºC dec⁻¹).

At 20 m depth, MAGT estimated showed a comparable long-term warming trend. In 1950, MAGT ranged from -3 to -2 ºC at the five observatories (Fig. 3 and 4). The strongest MAGT warming rate was recorded at Amsler (0.27 ± 0.01 ºC dec⁻¹), followed by King Sejong (0.24 ± 0.01 ºC dec⁻¹), SKO Station (0.22 ± 0.01 ºC dec⁻¹), Papagal (0.21 ± 0.01 ºC dec⁻¹), and Cierva (0.19 ± 0.01 ºC dec⁻¹) (Table 4).

Table 4: Rates of change of ground temperatures on the PERMANTAR observatories

Observatory	MAAT (ºC/decade)	MAGST (ºC/decade)	TTOP (ºC/decade)	MAGT (ºC/decade)
King Sejong	0.36±0.04	0.25±0.03	0.26±0.02	0.24±0.01
Papagal	0.33±0.04	0.21±0.03	0.22±0.02	0.21±0.01
SKO Station	0.34±0.04	0.22±0.03	0.23±0.02	0.22±0.01
Cierva	0.25±0.03	0.20±0.03	0.21±0.02	0.19±0.01
Amsler	0.36±0.05	0.27±0.04	0.29±0.02	0.27±0.01

https://doi.org/10.5194/egusphere-2026-1914
Preprint. Discussion started: 16 June 2026

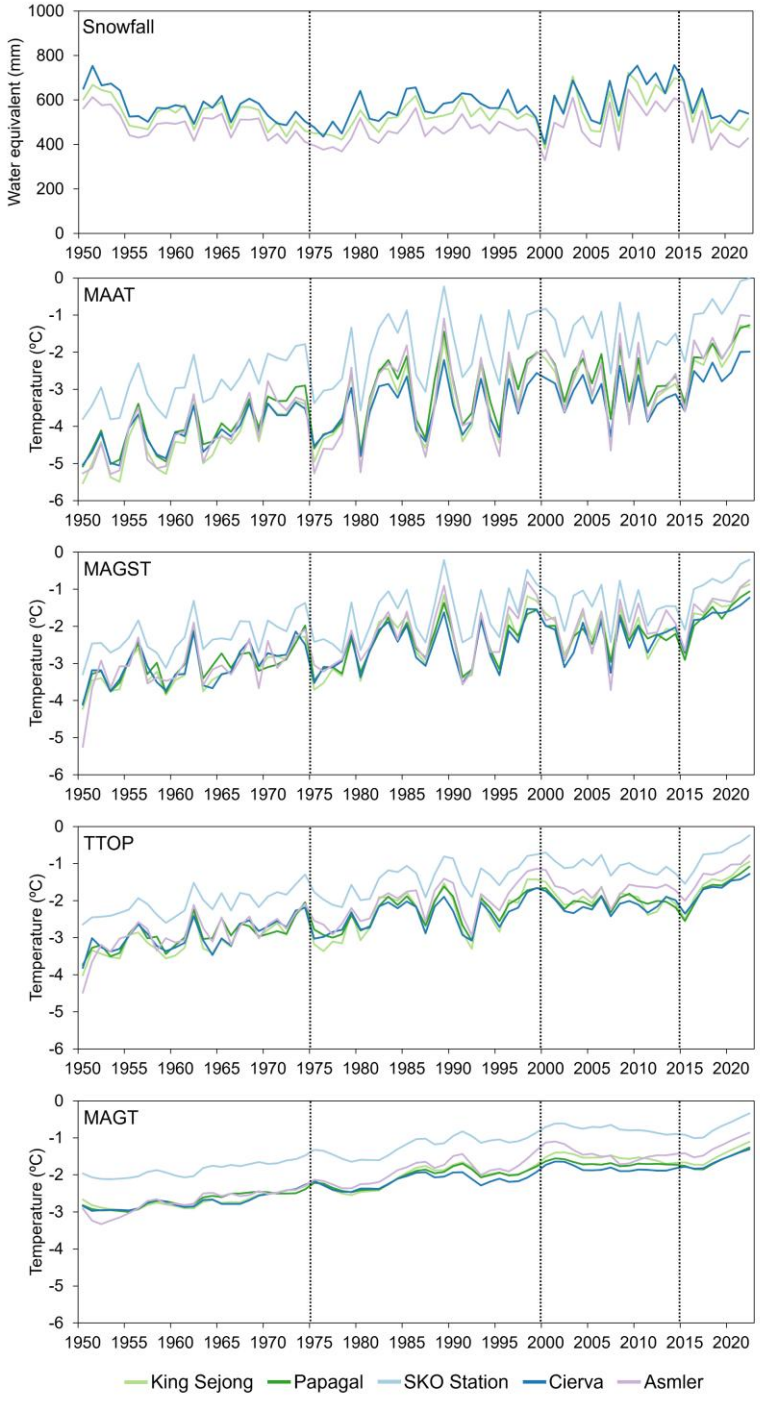

Figure 3: Long-term simulation of ground temperatures (January 1950 to December 2022) for the PERMANTAR observatories: snow water equivalent - SWE (mm), mean annual air temperature - MAAT (ºC); mean annual ground surface temperature - MAGST (ºC); temperature at the top of permafrost - TTOP (ºC); mean annual ground temperature at 20 m - MAGT (ºC).

https://doi.org/10.5194/egusphere-2026-1914
Preprint. Discussion started: 16 June 2026

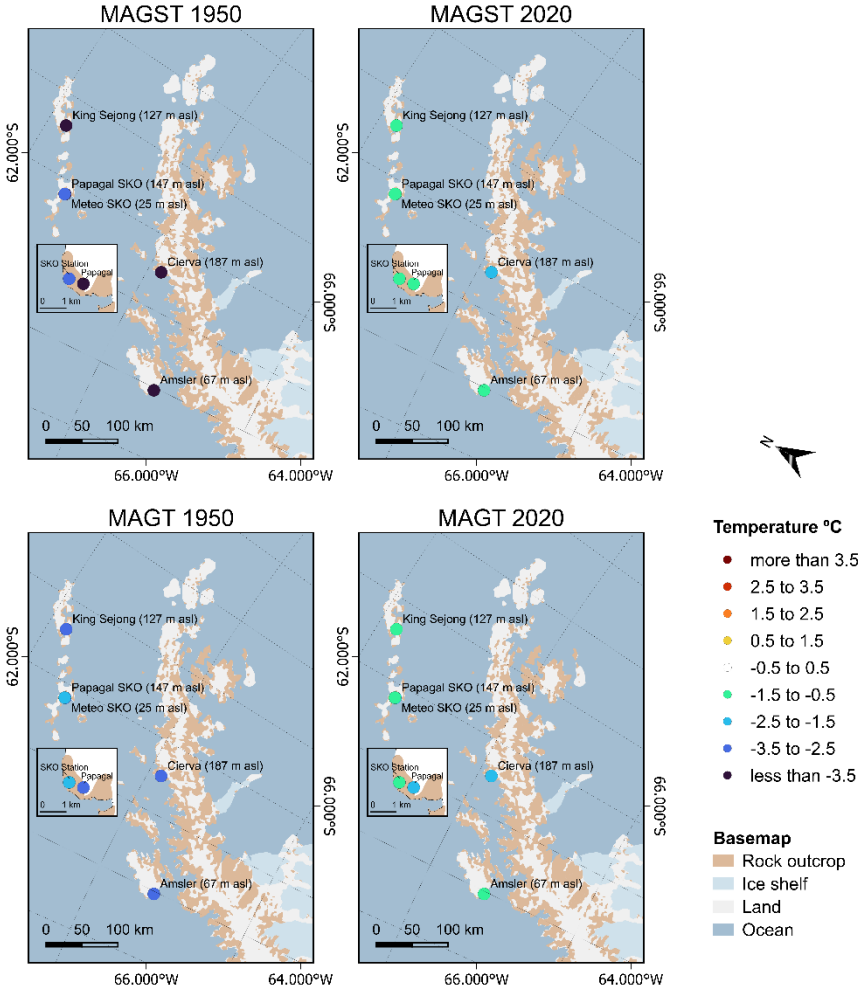

Figure 4: Mean annual ground surface temperature (MAGST) and mean annual ground temperature at 20 m depth (MAGT) simulated for the PERMANTAR observatories for 1950 and 2020. Basemap from Quantartica dataset (Matsuoka et al., 2018).

The distinctive periods identified are characterized by the interannual variability and short-duration trends (Fig. 3):

- *Period 1 (1950 - 1975)*: Between 1950 to 1975, a progressive warming trend is observed in both air (0.54 ± 0.1 ºC.dec^{-1}) and ground temperatures (MAGST, 0.36 ± 0.12 ºC.dec^{-1} and MAGT, 0.27 ± 0.03 ºC.dec^{-1}), accompanied by a reduction of the snowfall, with small interannual variability. This variability is marked by short periods of cooling with less snowfall (<500 mm SWE) and warming with more snowfall (>500 mm SWE), with a thermal amplitude of *c.* 2 ºC. The most pronounced cooling occurred around 1975, attributed to changes in circulation patterns and sea-ice conditions associated with the Amundsen Sea Low (ASL). MAGST and TTOP values were similar across most observatories, ranging from -5 to -2 ºC, except at SKO Station, where values were generally 1 ºC warmer. This

https://doi.org/10.5194/egusphere-2026-1914
Preprint. Discussion started: 16 June 2026

deviation was even more pronounced at 20 m depth with MAGT at SKO Station ranging from -2 to -1 ºC, while at the other observatories, values were ranging from -3 to -2 ºC.

- *Period 2 (1975 - 2000)*: From 1975 to 2000, alternating short warming and cooling periods became more intense, with MAAT variations exceeding 2 ºC, despite more constant snowfall values (500-600 mm water equivalent). This high variability led to strong variation in MAGST across the observatories, ranging from -4 to 0 ºC. This variation is also observed on TTOP, which ranged from -3 to -1 ºC. During this period, differences in permafrost temperatures at 20 m depth between the observatories became clearer, with warming rates bound in the upper limit by Amsler (0.34 ± 0.05 ºC.dec^{-1}) and in the lower by Cierva (0.16 ± 0.04 ºC.dec^{-1}). SKO Station followed the overall trend but consistently recorded higher MAGT values, above -2 ºC.

- *Period 3 (2000 - 2015)*: Between 2000 to 2015, the general warming trend in air temperatures was interrupted at all five observatories, by a short cooling period (-0.44 ± 0.30 ºC.dec^{-1}) followed by an increase in snowfall (>500 mm water equivalent). Despite continued interannual air temperature variability, MAGST fluctuated between -4 to -1 ºC. During this period, MAGT values, which ranged from -2 to -1 ºC, experienced a minor decrease that did not exceed 1 ºC.

- *Period 4 (2015 - 2022)*: The final years of the series were marked by intense and rapid warming (2.10 ± 0.60 ºC.dec^{-1}) and a general decrease of snowfall, when compared to the previous period. Air temperatures increase, lead to a sharp rise in MAGST from -3 to -2 ºC in 2015, to between -1 and -0.5 ºC by 2022, with a warming rate of 1.93 ± 0.40 ºC.dec^{-1}. Permafrost temperatures at 20 m depth also responded to this warming, with an increase rate of 0.90 ± 0.10 ºC.dec^{-1}.

4.3 Future evolution of permafrost temperature and active layer thickness under CMIP6 scenarios (2020 - 2100)

The simulation of ground temperatures until 2100 under the CMIP6 scenarios allowed us to project three outcomes for permafrost evolution (Fig. 5) and potential warming trends for the Northwestern Antarctic Peninsula (Table 5). We first examine the air temperature trends along the Antarctic Peninsula between 2020 and 2100 to provide context. We then analyze the evolution of MAGST and MAGT.

4.3.1 SSP1-2.6

Under the SSP1-2.6 scenario, an average warming of 0.59 ± 0.22 ºC is projected for the Northwestern Antarctic Peninsula for 2100. At the PERMANTAR observatories, the MAAT is expected to range between -1.4 and 0.5 ºC by 2100. Under this scenario, MAGST is projected to gradually warm at a rate of approximately 0.12 ± 0.03 ºC.dec^{-1}, diverging from the other scenarios through stabilization, particularly after 2040 (Fig. 5). Observatories with temperatures between -1.6 to -1.0 ºC in

https://doi.org/10.5194/egusphere-2026-1914
Preprint. Discussion started: 16 June 2026

2020 are expected to warm between -1.4 to 0.4 ºC, being the warming more pronounced at the northern observatories of SKO Station (0.14 ± 0.03 ºC.dec^{-1}), Papagal (0.13 ± 0.03 ºC.dec^{-1}) and King Sejong (0.11 ± 0.03 ºC.dec^{-1}), (Fig. 6).

MAGT at 20 m depth shows an average warming trend of 0.22 ± 0.01 ºC.dec^{-1} (Table 5). For most of the observatories, this warming rate will lead to positive MAGTs after 2090 at Papagal and after 2050 at SKO Station and Amsler (Fig. 5). King Sejong and Cierva are the only observatories with negative MAGTs estimates in 2100 (-0.1 and -0.8 ºC, respectively) (Fig. 6). These sites also exhibited the coldest MAGTs in 2020 (-2.2 and -2.7 ºC), compared with Papagal, SKO Station, and Amsler (-2.1, -1.1, and -1.6 ºC) (Fig. 6).

At an intermediate depth of 10 m, the five observatories are estimated to have permafrost. However, the maximum annual ground temperature at 10 m becomes positive as early as 2034 at SKO Station and Amsler, in 2068 at Papagal, and in 2091 at King Sejong, while it remains negative at Cierva (Appendix E and Fig. E1). Additionally, ground temperatures at this depth exhibit more pronounced interannual variability, reflecting the influence of surface conditions.

4.3.2 SSP2-4.5

Under the SSP2-4.5 scenario, a more pronounced warming is projected, with an average rate of 2.59 ± 0.20 ºC across the Northwestern Antarctic Peninsula (Fig. 5 and Table 5). At the PERMANTAR observatories, MAAT values ranging from -1.3 to 0 ºC in 2020, are projected to increase to 1.3-2.7 ºC by 2100.

In this warming scenario, MAGST is estimated to have a stronger warming trend of 0.38 ± 0.02 ºC.dec^{-1} on the PERMANTAR observatories (Fig. 5 and Table 5). Consequently, MAGST values will vary between 1.3 to 2.6 ºC by 2100, with a maximum difference of 4 ºC to the values obtained for 2020 (Amsler) (Fig. 6).

MAGT at 20 m depth is projected to warm by 0.35 ± 0.01 ºC.dec^{-1} (Fig. 5 and Table 5). This warming trend suggests that, consistent with historical patterns, the actual environmental conditions promote a progressive warming of permafrost, leading to gradual degradation. By 2100, MAGT is projected to be positive at the five observatories, ranging from 0.6 ºC to 2.2 ºC (Fig. 5 and 6). It is noticed that the observatories located further south exhibit more pronounced warming rates, with 0.36 ± 0.01 ºC.dec^{-1} at Cierva and 0.43 ± 0.01 ºC.dec^{-1} at Amsler, compared to rates between 0.31 ± 0.01 ºC.dec^{-1} and 0.34 ± 0.01 ºC.dec^{-1} at the remaining sites (Table 5). This pronounced warming can be enhanced at Cierva by the higher snow factor used (50%) which suggests a stronger insulating effect that prevents the cooling of the ground during the freezing season and can hasten the warming. Additionally, the sheltered location diminishes the influence of prevailing moist frontal systems reaching from west, that could reduce the cooling effect. At Amsler, rather than a sheltered location, the low elevation (67 m asl) and the higher snow factor used (50%) appears to be determinant for the stronger warming rate.

At a depth of 10 m, positive MAGT values are estimated to occur 20 years earlier (between 2028 and 2068) than at 20 m (between 2050 and 2077) (Appendix E and Fig. E1).

https://doi.org/10.5194/egusphere-2026-1914
Preprint. Discussion started: 16 June 2026

4.3.3 SSP5-8.5

Under the SSP5-8.5 scenario, an average warming of 5.05 ± 0.2 ºC is foreseen for the Northwestern Antarctic Peninsula. By 2100, MAAT at the PERMANTAR observatories is expected to range from 4 to 5 ºC. The spatial differences suggest a more pronounced warming while approaching the southern latitudes of the Western Antarctic Peninsula. In line with this, MAGST is projected to increase at an average rate of 0.66 ± 0.02 ºC.dec^{-1}, reaching values between 4 to 5 ºC by 2100 (Fig. 5 and Table 5). The higher values around 5 ºC are estimated for the observatories at lower elevation such as SKO Station (25 m asl) and Amsler (67 m asl), while the values around 4 ºC are estimated for the observatories at higher altitude such as Papagal (147 m asl) and Cierva (187 m asl), or with the lowest snow factor alike King Sejong (30%) (Fig. 6).

This prolonged surface warming propagates to deeper layers, leading to permafrost warming and degradation (Fig. 8). The warming rate at depth follows the same pattern observed for MAGST, with higher warming rates at lower latitudes (Table 5). Therefore, at Amsler a rate of 0.62 ± 0.01 ºC.dec^{-1} is estimated against a rate of 0.46 ± 0.01 ºC.dec^{-1} at King Sejong.

As a consequence of the intense warming at the southern observatories, MAGT at 20 m depth is expected to be positive by 2045 at Amsler where temperatures are projected to reach 3.7 ºC by 2100 (Fig. 5 and 6). At Cierva despite a warming rate of 0.51 ± 0.01 ºC.dec^{-1} positive MAGT is projected to 2071 (Fig. 5 and Table 5). By 2100, estimated MAGT is of 2 ºC (Fig. 6). With the exception of SKO Station where MAGT is already positive by 2045, due to the higher temperature values, King Sejong and Papagal are expected to have positive MAGTs at 20 m depth around 2060 and reach a MAGT of 2 ºC by 2100 (Fig. 5 and 6).

At a depth of 10 m, positive MAGT values are estimated to occur 15 years earlier (between 2029 and 2057) than at 20 m (between 2045 and 2071) (Appendix E and Fig. E1).

Table 5: Change rates of ground temperatures at 20 m depth on the PERMANTAR observatories from 2020 to 2100.

Observatory	MAAT (ºC/decade)			MAGST (ºC/decade)			MAGT (ºC/decade)		
	ssp1-2.6	ssp2-4.5	ssp5-8.5	ssp1-2.6	ssp2-4.5	ssp5-8.5	ssp1-2.6	ssp2-4.5	ssp5-8.5
King Sejong	0.08±0.02	0.29±0.02	0.58±0.02	0.11±0.03	0.34±0.02	0.61±0.02	0.23±0.01	0.31±0.01	0.46±0.01
Papagal	0.09±0.03	0.31±0.02	0.61±0.02	0.13±0.03	0.37±0.02	0.64±0.02	0.23±0.01	0.33±0.01	0.48±0.01
SKO Station	0.10±0.03	0.32±0.02	0.62±0.02	0.14±0.03	0.38±0.02	0.66±0.02	0.21±0.01	0.34±0.00	0.51±0.01
Cierva	0.06±0.03	0.34±0.03	0.65±0.02	0.10±0.03	0.40±0.02	0.68±0.02	0.23±0.01	0.36±0.01	0.52±0.01
Amsler	0.05±0.03	0.35±0.03	0.68±0.02	0.10±0.03	0.42±0.03	0.72±0.02	0.23±0.01	0.43±0.01	0.62±0.01

https://doi.org/10.5194/egusphere-2026-1914
Preprint. Discussion started: 16 June 2026

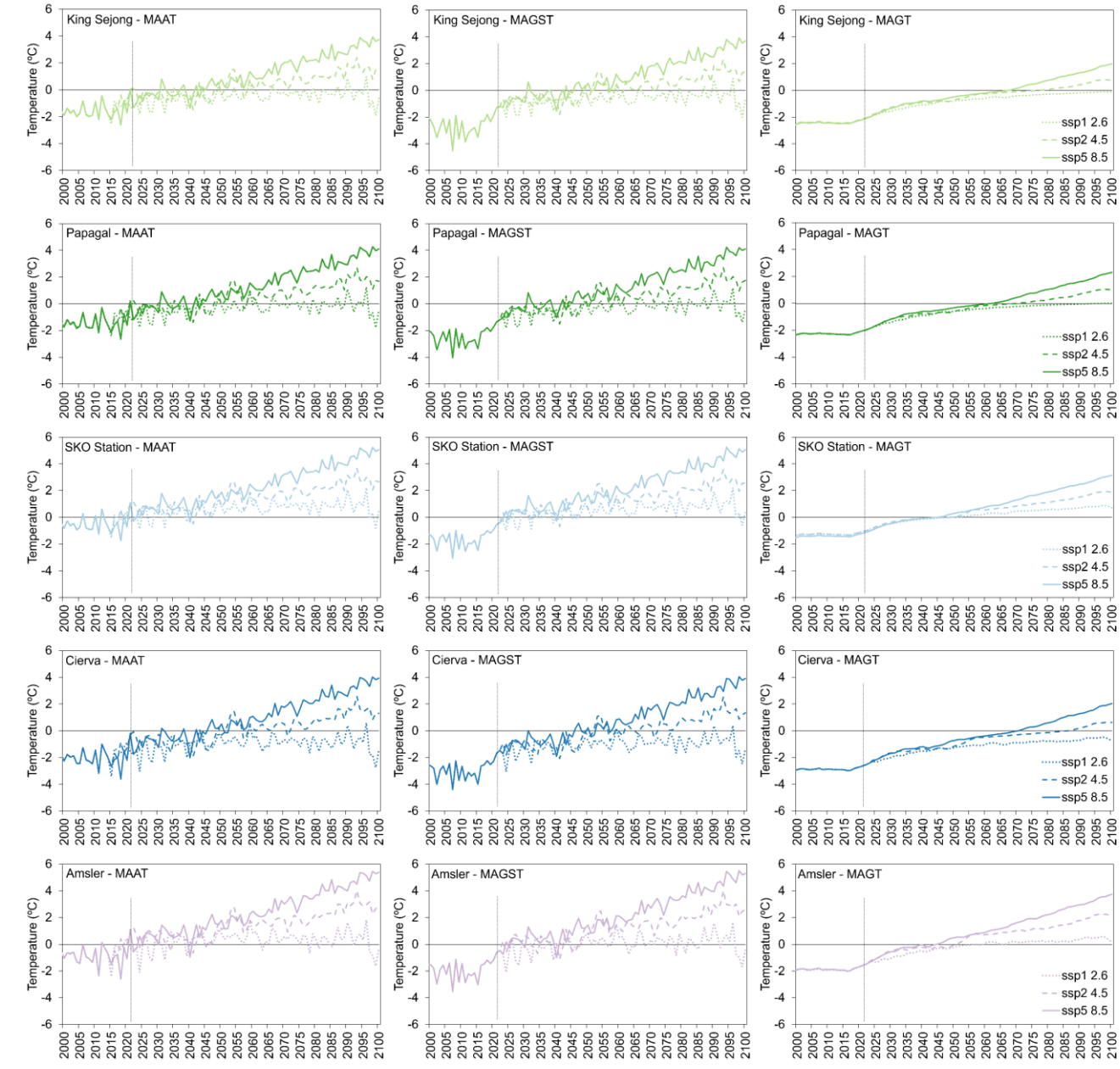

Figure 5: Long-term simulation of ground temperature (2022 - 2100) on PERMANTAR observatories: mean annual air temperature - MAAT (°C); mean annual ground surface temperature - MAGST (°C); mean annual ground temperature at 20 m depth - MAGT (°C).

https://doi.org/10.5194/egusphere-2026-1914
Preprint. Discussion started: 16 June 2026

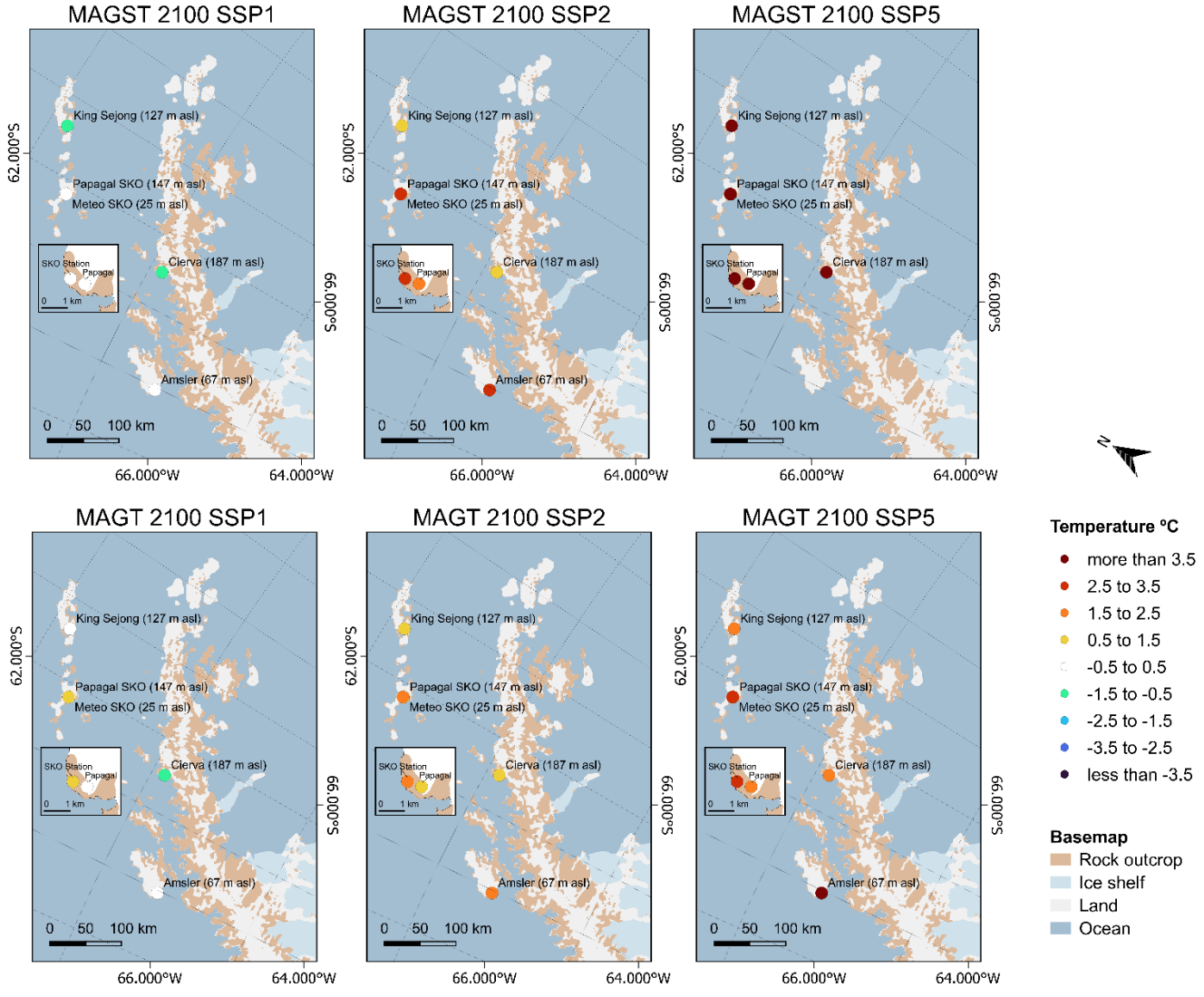

Figure 6: Mean annual ground surface temperature (MAGST) and mean annual ground temperature (MAGT) at 20 m depth on PERMANTAR observatories in 2100 under the SSP1, SSP2 and SSP5 CMIP6 scenarios. Basemap from Quantartica dataset (Matsuoka et al., 2018).

https://doi.org/10.5194/egusphere-2026-1914
Preprint. Discussion started: 16 June 2026

5 Discussion

5.1 Past evolution of permafrost temperature (1950 - 2020)

The simulated past evolution of permafrost temperature forced by the ERA5 data provided an overview of the ground thermal regime across the PERMANTAR observatories in the Antarctic Peninsula since 1950. The results revealed a general warming trend in MAAT (0.33 ºC.dec^{-1}), with an acceleration after 2016. This agrees with the warming trend also reported by Carrasco et al. (2021), for the evolution of the air temperature in the Antarctic Peninsula considering both the western region and colder eastern region, where an overall warming trend of 0.26 ºC.dec^{-1} was presented for the period from 1978 to 2020. The same authors, for Vernadsky Station (65.24 ºS), about 50 km south of Amsler, report a warming rate of 0.45 ºC.dec^{-1} (1951-2020), being close to the warming rate of 0.36 ± 0.05 ºC.dec^{-1} that we simulated for Amsler.

The differences in the calculated warming rates of the MAGST, TTOP, and MAGT are mainly controlled by local settings. The low altitude and short duration of the snow cover, influenced by the exposition to the wind and topography, were the main factors determining a stronger warming rate on the southernmost observatory of Amsler (MAGST, 0.27 ± 0.04 ºC.dec^{-1} and MAGT, 0.27 ± 0.01 ºC.dec^{-1}), followed by the northernmost, King Sejong (MAGST, 0.25 ± 0.03 ºC.dec^{-1} and MAGT, 0.24 ± 0.01 ºC.dec^{-1}). In contrast, at Cierva and Papagal, higher elevations and a more persistent snow cover appear to buffer the regional warming signal, resulting in comparatively lower ground-temperature warming trends (MAGST, 0.20 ± 0.03 ºC.dec^{-1} and 0.21 ± 0.03 ºC.dec^{-1}; MAGT, 0.19 ± 0.01 ºC.dec^{-1} and 0.21 ± 0.01 ºC.dec^{-1}).

Ground temperatures reflect both long-term climatic trends and short-term variability. The initial warming period (1950-1975) coincides with increasing MAAT and decreasing snowfall, favoring higher ground temperatures and relatively small interannual variability. Then, an increased interannual MAAT variability of 2 ºC led to a wider range of MAGST and TTOP values. The cooling recorded between 2000 and 2015, together with increased snowfall, produced a reduction in MAGT (<1 ºC). This period is followed by intense atmospheric warming and reduced snowfall, which induced a rapid increase in MAGST and a pronounced response at depth, with MAGT warming rates up to 0.90 ± 0.10 ºC dec. The increase of MAGTs towards −1 and −0.5 ºC suggests that permafrost is approaching a thermal state that under continued atmospheric warming, can lead to degradation.

5.2 Future evolution of permafrost temperature (2022 - 2100)

The simulations forced with the CMIP6 model in different scenarios allowed the development of permafrost temperature projections until 2100 for the PERMANTAR observatories in the Northwestern Antarctic Peninsula. In the three CMIP6 scenarios, the evolution of the MAAT, MAGST and MAGT exhibit two similar periods prior to the divergence into distinct warming trends. The first period extends from 2000 until 2015, during which temperatures show interannual variability and a small cooling as in observational data. This is followed by a second period, from 2016 to 2040, characterized by a rapid increase in temperature. The initial years of this period (2016-2022) correspond to a phase of intensified warming marked by

https://doi.org/10.5194/egusphere-2026-1914
Preprint. Discussion started: 16 June 2026

several warm weather episodes documented by González-Herrero et al. (2022) and Gorodetskaya et al. (2023). The warming projected for the subsequent two decades is consistent with that reported by Zhu et al. (2025) in their analysis of extreme temperature indices over Antarctica under the CMIP6 scenarios. The authors report that the projected warming results from climate system inertia and existing radiative forcing that would delay the warming caused by the concentration of GHG already emitted (Zhu et al., 2025). Additionally, the climate response until 2040 includes the polar amplification mechanisms and ocean-sea ice interaction dynamics that amplify warming (Morioka et al., 2024).

From 2040 onward, warming trends diverge among the scenarios, in accordance with their respective emission pathways. Under SSP1-2.6, temperatures tend to stabilize, whereas SSP2-4.5 maintains a gradual warming trend and SSP5-8.5 indicates an accelerated temperature increase toward 2100. Among these scenarios, SSP2-4.5 is considered an intermediate pathway, representing a continuation of current socio-economic trends. Over the Antarctic continent, several studies have analyzed future climate conditions under this scenario, reporting a consistent warming trend. According to Sun et al. (2025), the SSP2-4.5 emission scenario is projected to result in Antarctic warming at a rate of 0.28 ºC dec^{-1}. This continental-scale warming rate is lower than that estimated for the Northwestern Antarctic Peninsula (0.32 ± 0.02 ºC dec^{-1}).

Under the more optimistic SSP1-2.6 scenario, the projections indicate a MAAT warming rate of 0.59 ± 0.22 ºC over the Northwestern Antarctic Peninsula, resulting in an increase in permafrost temperature at all observatories, with ground warming rates of approximately 0.22 ± 0.01 ºC dec^{-1}. Consequently, by 2100, negative MAGT at 20 m depth are projected to persist only at King Sejong and Cierva, although with temperatures above −1 ºC. At the remaining sites, positive MAGTs at 20 m are projected to occur by 2080.

Following the historical trend, the SSP2-4.5 scenario estimates a much stronger MAAT warming rate of 2.59 ± 0.20 ºC. Consequently, MAGT at 20 m depth exhibits a more accelerated warming, leading to positive MAGTs at 20 m depth at all five observatories by 2087, with values ranging from 1 to 2 ºC. In contrast to the SSP1-2.6 scenario, SSP2-4.5 displays a distinct spatial pattern in MAAT warming rates, with increased warming at the more southerly observatories which may be related to the sea ice loss on the Bellingshausen Sea and consequent deepening of the ASL that strengthens north-northwesterly flow towards the Antarctic Peninsula, favoring advection of warm, maritime air and raising surface air temperatures, especially during the winter (Abram et al., 2010; Turner et al., 2013). This is further amplified by the low elevation of the Amsler observatory, that shows a simulated severe warming (0.43 ± 0.01 ºC.dec^{-1}), and positive MAGT by 2051, following the low elevation SKO Station where positive MAGT is predicted for 2049. On Papagal, positive MAGT is expected by 2071 followed by King Sejong (2077) and Cierva (2087).

Under SSP5-8.5 (MAAT warming of 5.05 ± 0.18 ºC) permafrost degradation occurs more rapidly, with positive MAGTs at 20 m depth emerging 6 to 16 years earlier than under SSP2-4.5. The timing of this transition is also influenced by the initial MAGT values. Amsler, with a MAGT of −1.7 ºC in 2020 and a warming rate of 0.62 ± 0.01 ºC.dec^{-1}, is expected to record a positive MAGT at 20 m depth by 2045. SKO Station, with a MAGT of -1.1 ºC in 2020 and a warming rate of 0.51 ± 0.01

https://doi.org/10.5194/egusphere-2026-1914
Preprint. Discussion started: 16 June 2026

ºC.dec⁻¹, by 2045 followed by King Sejong and Papagal in 2060, which had MAGTs of −2.0 ºC in 2020, and warming rates of 0.46 and 0.48 ± 0.01 ºC dec⁻¹, respectively. Cierva, with a MAGT of −2.7 ºC in 2020 and the second-highest warming rate (0.52 ± 0.01 ºC dec⁻¹), is projected to have positive MAGT at 20 m depth by 2071.

6 Conclusions

The implementation of the CCM forced by ERA5 data demonstrated that it enabled an adequate representation of the environmental conditions and associated ground temperatures at the PERMANTAR observatories. The bias calculated from measured and simulated ground temperatures was below 1 ºC, highlighting the model's capacity for estimating ground temperatures. Moreover, the application of reanalysis data and CMIP6 projections as forcing, allowed for modelling the evolution of the recent past and future permafrost conditions, providing an overview of the long-term ground thermal regime in the Northwestern Antarctic Peninsula.

The simulation of permafrost evolution since 1950 revealed a general warming trend across all observatories, which intensified after 2016 following increases in both the frequency and intensity of warm extremes. This warming was more pronounced at the southernmost site (Amsler, 67 m asl), where MAGT increased at 0.27 ± 0.01 ºC dec⁻¹, followed by King Sejong (127 m asl), with a rate of 0.24 ± 0.01 ºC dec⁻¹ and by the lowest site (SKO Station, 25 m asl), associated to already relatively warm conditions, with a rate of 0.22 ± 0.01 ºC dec⁻¹ .

The simulation of the future evolution of ground temperatures indicates a consistent warming trend across the three scenarios, even in SSP1-2.6, suggesting that extensive permafrost degradation is expected to occur at low altitude across the Northwestern Antarctic Peninsula by 2100.

Under the SSP2-4.5 scenario, with a MAAT warming rate of 2.59 ± 0.20 ºC, an intense warming and degradation of permafrost is predicted, which is more severe in the southern observatories, resulting in positive MAGTs at 20 m depth from 2051 to 2087. This is possibly due to the reduction of sea ice on the Bellingshausen Sea and consequent deepening of the ASL that contributes to the advection of warm, maritime air and to the increase of temperatures during the winter (Abram et al., 2010; Turner et al., 2013).

In the worst-case scenario (SSP5-8.5), with a warming of the Northwestern Antarctic Peninsula of 5.05 ± 0.18 ºC by 2100, MAGTs at 20 m depth will start to be positive already in 2045 in most observatories and by 2071 in all the observatories, reaching 2 to 4 ºC by 2100.

Our results demonstrate that the future projected warming across the Northwestern Antarctic Peninsula, independently of the CMIP6 scenario will very likely lead to the loss of permafrost from coastal areas and low elevation sites. Such major changes in ground thermal state will modify surface and subsurface hydrology, biogeochemical fluxes and geomorphological processes, with implications for the sensitive terrestrial (and potentially also to nearshore) ecosystems, and exposing human infrastructure

https://doi.org/10.5194/egusphere-2026-1914
Preprint. Discussion started: 16 June 2026

(research stations, roads, and airstrips) to degradation. Similarly to what is recorded in comparable regions in the Arctic, in non-consolidated deposits, thermokarst and landslide activity should increase. In the steep rocky slopes, so typical of the coastal areas of the Northwestern Antarctic Peninsula, as bedrock warms and thaw propagates along joints, rockfalls and landslides may become more frequent, increasing hazards in areas that are experiencing growing tourist visitation during the austral summer.

https://doi.org/10.5194/egusphere-2026-1914
Preprint. Discussion started: 16 June 2026

Appendix A: Description of PERMANTAR monitoring sites

This appendix provides information on the five PERMANTAR observatories selected for this study, including site descriptions, instrumentation setup over time, and the accuracy of the sensors used.

The **King Sejong Observatory** (62.228883 ºS, 58.770317 ºW) was installed in March 2019. It consists of a 13 m depth borehole drilled in an andesite spur in Jeonjaegyu valley at 127 m asl, and of an air temperature logger. Located at the edge of an incipient glacial cirque, has in the surrounding area extensive frost shattered debris, with the formation of active stone circles and solifluction lobes (Baptista et al., 2024; López-Martínez et al., 2012). Ground temperature data is recorded hourly using a Geoprecision M-Log5W-String datalogger (accuracy ±0.1 ºC) with a string of 15 temperature digital sensors down to 13 m depth. GST is monitored using a Geoprecision M-Log5W-Cable datalogger (accuracy ±0.1 ºC) buried at 2 cm depth. Air temperature is recorded using a similar logger inside a radiation shield at 1.5 m above the ground.

The **Papagal Observatory** (62.648389 ºS, 60.363694 ºW) was installed in 2008. At the site a 4 m deep borehole was drilled in a quartzite outcrop at 147 m asl. The observatory also includes one air temperature logger and a ground surface temperature logger. The observatory is located in a flat interfluve covered by frost-shattered debris near Papagal Peak, at the margin of Hurd Glacier. Due to its longer operational period, several instrument configurations have been used. From 2008 to 2018 Thermochron iButtons DS1922L (accuracy ±0.125 ºC, (Gubler et al., 2011)) were installed as well as for GST, with temperature readings taken every 4 hours. Air temperatures were recorded using TinyTag Plus loggers with PT1000 (accuracy ±0.1 ºC). In 2018, the system was upgraded with a Geoprecision M-Log5W-String datalogger (accuracy ±0.1 ºC) with 8 sensors down to 4 m depth, and two Geoprecision M-Log5W-Cable dataloggers (accuracy ±0.1 ºC) for air and GST, all set to record at 1-hour intervals.

The **St Kliment Ohridski (SKO) Station Observatory** (62.64142 ºS, 60.36397 ºW), was installed in 2009 in a rock knob southeast of the Bulgarian Station Saint Kliment Ohridski. It includes an 8 m deep borehole drilled in a quartzite outcrop at 25 m asl, an air temperature and a GST logger. From 2009 to 2018 HOBO Pendant Temperature Data Loggers (accuracy ±0.5 ºC) were used. GST was monitored using a Thermochron iButton DS1922L. Air temperature was monitored using Tinytag Plus loggers. In 2018, this system was replaced by a Geoprecision M-Log5W-String datalogger with 12 sensors down to 8 m depth, and Geoprecision M-Log5W-Cable dataloggers for air and GST, all recording hourly.

The **Cierva Observatory** (64.16195 ºS, 60.950933 ºW) was installed in 2012 on the Cierva's Point slope facing north-northwest, at 187 m asl. It includes a 15 m deep borehole drilled in a granodiorite outcrop, a meteorological station (Campbell), and a GST logger. Initially, ground temperatures were monitored using Thermochron iButtons DS-1922L at a 4-hour interval. In 2015 the system was upgraded with a Geoprecision M-Log5W-String datalogger with 18 sensors down to 15 m depth, and a Geoprecision M-Log5W-Cable datalogger for GST recording hourly.

https://doi.org/10.5194/egusphere-2026-1914
Preprint. Discussion started: 16 June 2026

The **Amsler Observatory** (64.761533 ºS, 64.07425 ºW) was installed in 2012 in a granite rock outcrop in a gentle surface close to the summit of the highest hill of Amsler Island at 67 m asl. The original borehole was 14 m deep, equipped with Thermochron iButtons DS1922L. In 2014 the lower 5 m of the borehole were lost. Since 2017 a Geoprecision M-Log5W-String datalogger is used with 13 temperature sensors down to 9 m depth. In 2023 an air temperature and a GST logger (Geoprecision M-Log5W-Cable) were installed, recording hourly.

Figure A1: General setting of the PERMANTAR boreholes analyzed in this study.

https://doi.org/10.5194/egusphere-2026-1914
Preprint. Discussion started: 16 June 2026

Appendix B: Comparison between ERA5-derived air temperature and in situ measurements at the PERMANTAR observatories.

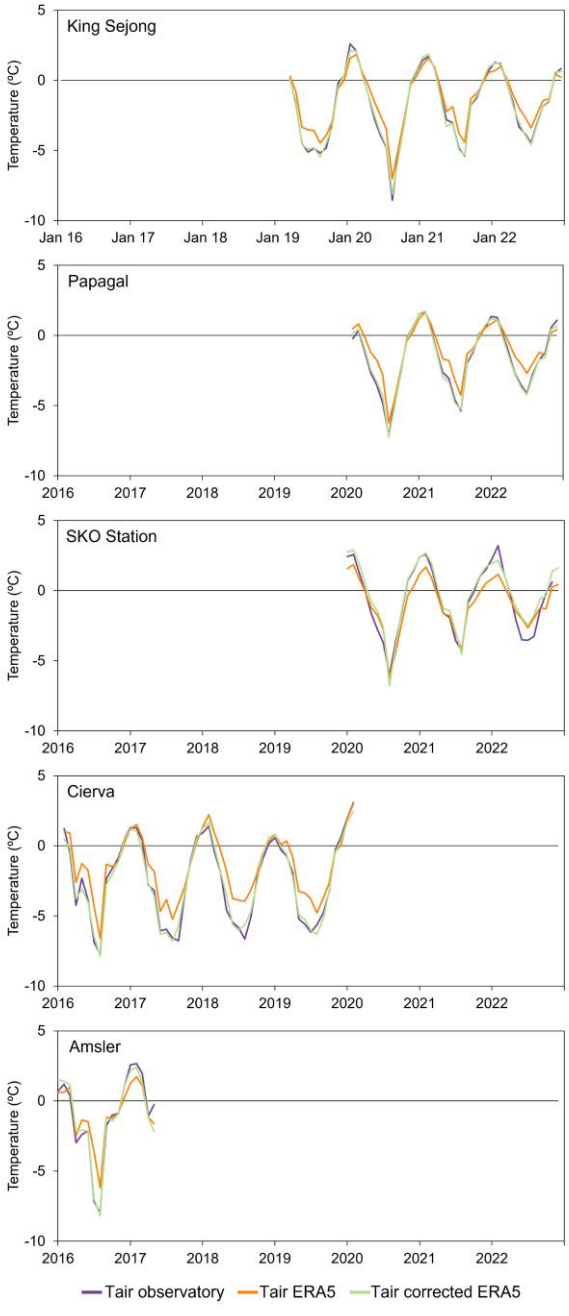

Figure B1: Comparison between mean monthly air temperatures recorded at the PERMANTAR observatories, ERA5-derived and ERA5-derived bias corrected.

https://doi.org/10.5194/egusphere-2026-1914
Preprint. Discussion started: 16 June 2026

Appendix C: Evaluation of CMIP6 models

This appendix provides context on the application of the three CMIP6 models in Antarctica and presents the results of the evaluation performed.

Regarding the context, Bozkurt et al. (2024) when analyzing atmospheric blocking patterns over the Antarctic Peninsula for a historical (1981-2010) and future (2071-2100, SSP5-8.5) periods using ERA5 reanalysis and six CMIP6 models, showed that there are marked differences between the CMIP6 ensemble and ERA5, especially during austral winter. Among the models, INM-CM4-8 reproduced key spatial patterns and temperature anomalies relatively well, particularly in summer (December-February) and capture enhanced near-surface warming during winter (June-August).

Caillet et al. (2024) characterized the atmospheric and oceanic internal climate variability in a selection of three CMIP6 models, including the IPSL-CM6A, and estimated the impact on the Antarctic contribution to sea level over the 21st century under the SSP2-4.5 scenario. They concluded that atmospheric internal climate variability is similar in the three CMIP6 models, while the amplitude of oceanic internal climate variability around Antarctica strongly depends on the model. However, IPSL-CM6A, have arranged iceshelf melting vertically distributed to mimic the presence of unresolved ice-shelf cavities, important for coastal ocean properties around Antarctica (Mathiot et al., 2017). The IPSL-CM6A exhibited a realistic temperature profile in the Amundsen Sea.

Tewari et al. (2022) examined 38 CMIP6 models over Antarctica, aiming to evaluate the capacity to reproduce the climate through the surface temperature and precipitation, to better understand the robustness of the projections. An historical period (1950-2005) was used to calculate the pattern correlation coefficient and RMSE. Of the ten best performing models, the study identifies the ACCESS-CM2 model which, regarding the precipitation, lies within the range of ± 20% of the ERA5 (Tewari et al., 2022). Concerning the surface temperature, at a global scale, Rashid et al. (2022) in the evaluation of historical simulations (1850-2014) indicate that the model's simulation of surface temperature is similar to or better than the majority of other CMIP6 models when analyzing the Taylor diagram and the associated statistics. Schroeter et al. (2024) on the projection of future climate mention that the higher sensitivity of the ACCESS-CM2 allows to represent the amplified polar warming (APW), associated with the disintegration of the ice-sheet, and the seasonal asymmetries of the surface temperature. The APW is the outcome of the improved coupled between the ocean and ice on the model, mentioned by Kiss et al. (2020) whom obtained a close match between the modelled and observational estimates of ice-extent in Antarctica between 1993 and 2017.

Using the period 1950-2022 as a reference, the MAATs from the three CMIP6 models downscaled to the Papagal observatory location were compared against ERA5 reanalysis data to evaluate their performance in representing the climate conditions of the Western Antarctic Peninsula region (Fig. C1 and Table A1). Among the models, ACCESS-CM2 shows warmer values than ERA5, a MAE of 1.16 ºC, a RMSE of 1.33 ºC. and a standard deviation (σ) of 0.98, close to ERA5 (σ = 1.01). The INM-CM4-8 model overlaps with ERA5 MAATs but misrepresents interannual variability, with a lower σ of 0.78. The MAE is of 0.74 ºC and RMSE of 0.84 ºC. In contrast, the IPSL-CM6A model overestimates temperatures by up to 5 ºC in some years

https://doi.org/10.5194/egusphere-2026-1914
Preprint. Discussion started: 16 June 2026

(e.g. 2011-2013) and shows a MAE of 1.37 ºC and a RMSE of 2.81 ºC. However, this model also captures interannual variability and presents a higher σ of 1.49.

Linear trend indicates that ACCESS-CM2 simulates a warming trajectory of 0.36 ºC.dec^{-1}, closer to ERA5 (0.33 ºC.dec^{-1}), while IPSL-CM6A estimates a stronger warming of 0.44 ºC.dec^{-1}. In contrast, INM-CM4-8 predicts a much weaker warming of 0.15 ºC.dec^{-1}.

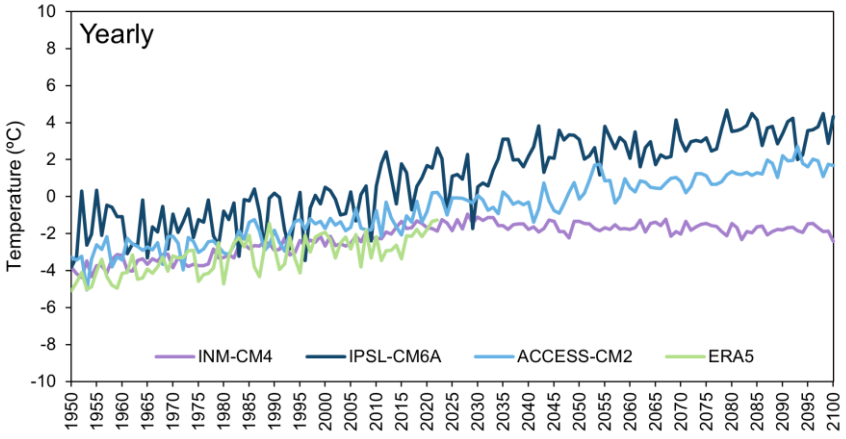

Figure C1: Mean annual air temperatures estimated for the Papagal observatory (Livingston Island) for 1950 - 2100. Comparison of the CMIP6 models INM-CM4-8, IPSL-CM6A and ACCESS-CM2 (scenario SSP2 4.5) and the ERA5 reanalysis.

Table C1: Comparison of CMIP6 models INM-CM4-8, IPSL-CM6-A and ACCESS-CM2 against ERA5 for the Papagal observatory (1950-2022).

Reanalysis/ Model	Linear trend ºC per decade	ERA5 – Model	
		MAE	RMSE
ERA5	0.33		
INM-CM4-8	0.15	0.74	0.84
IPSL-CM6-A	0.44	1.37	2.81
ACCESS-CM2	0.36	1.16	1.33

The difference between the air temperature represented by each model strongly impacts the simulation of ground temperatures, leading to markedly different permafrost thermal regimes and future trajectories. In this study, ACCESS-CM2 was selected to force the simulations of future permafrost evolution because it shows the best overall performance against ERA5, combining a similar linear trend and a realistic representation of interannual variability.

https://doi.org/10.5194/egusphere-2026-1914
Preprint. Discussion started: 16 June 2026

Appendix D: Simulated and observed ground temperatures on the five PERMANTAR observatories

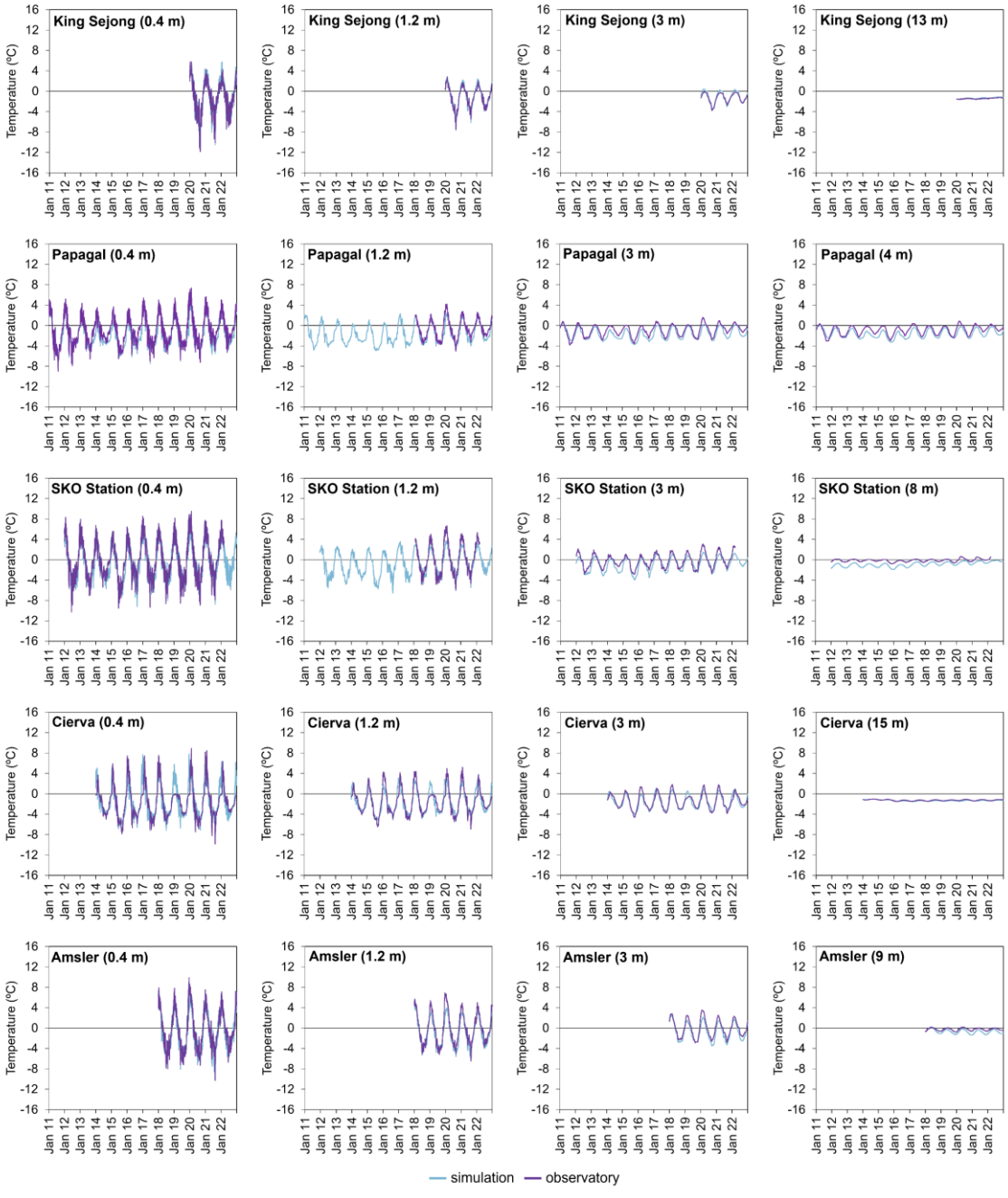

Figure D1: Comparison between simulated and observed ground temperatures at 0.4, 1.2, 3 and maximum borehole depth on the five PERMANTAR observatories selected.

https://doi.org/10.5194/egusphere-2026-1914
Preprint. Discussion started: 16 June 2026

Appendix E: Long-term simulation of ground temperature (2022 - 2100) on PERMANTAR observatories

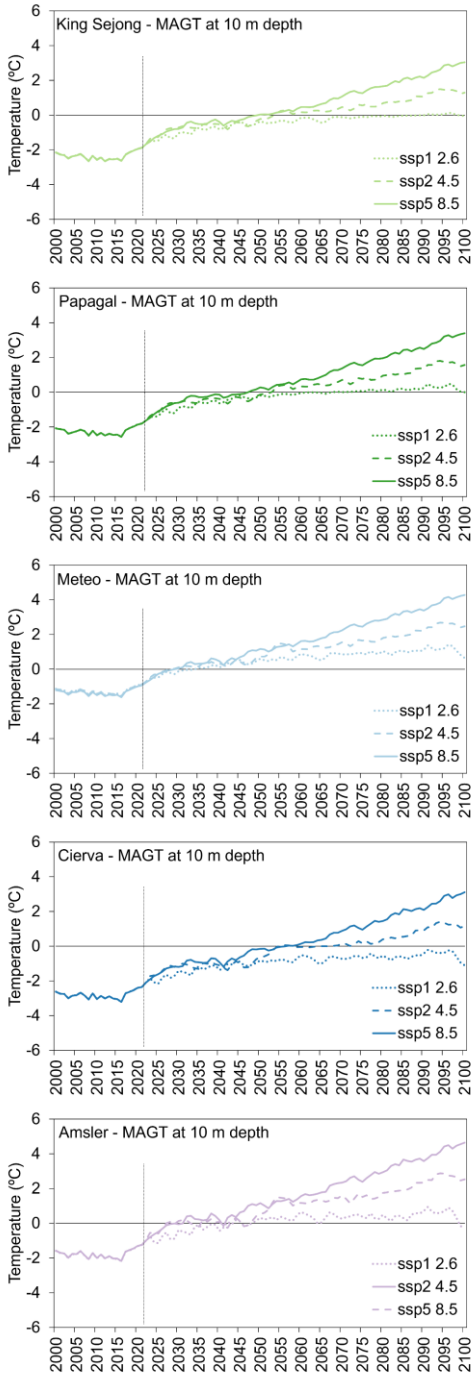

Figure E1: Mean annual ground temperature at 10 m depth (ºC).

https://doi.org/10.5194/egusphere-2026-1914
Preprint. Discussion started: 16 June 2026

Code availability

The current version of the model is available at https://github.com/CryoGrid/CryoGridCommunity_run

Data availability

The parameter files and forcing data used in this study will be made available at Zenodo after the manuscript acceptance. The data presented on the past and future evolution will be made available at Zenodo after the manuscript acceptance.

Author contributions

JB, SW and GV conceptualized the study; JB and GV collected data from the PERMANTAR observatories; JB and SW worked on the modelling implementation; GV secured financial support for the project; SW developed the software; SW and GV supervised the study; JB drafted the manuscript; and SW and GV reviewed the manuscript.

Competing interests

The contact author has declared that none of the authors has any competing interests.

Acknowledgements

The Portuguese Polar Program (PROPOLAR), the Korea Polar Research Institute (KOPRI), the Spanish Antarctic Program, the Bulgarian Antarctic Institute (BAI) and the team from the NSF Palmer Station are thanked for the logistical support. The ESA Permafrost_cci project (grant no. 4000123681/18/I-NB) is thanked for the support provided for the model implementation.

Financial support

This research has been supported by the Fundação para a Ciência e a Tecnologia (grant nos. 2022.06628.PTDC, 2021.05119.BD) and the European Space Agency (grant no. 4000123681/18/I-NB).

https://doi.org/10.5194/egusphere-2026-1914
Preprint. Discussion started: 16 June 2026

References

Abram, N. J., Thomas, E. R., McConnell, J. R., Mulvaney, R., Bracegirdle, T. J., Sime, L. C., and Aristarain, A. J.: Ice core evidence for a 20th century decline of sea ice in the Bellingshausen Sea, Antarctica, J. Geophys. Res., 115, 2010JD014644, https://doi.org/10.1029/2010JD014644, 2010.

Baptista, J., Vieira, G., and Lee, H.: Ground surface temperature regimes are controlled by the topography and snow cover in the ice-free areas of Maritime Antarctica, CATENA, 240, 107947, https://doi.org/10.1016/j.catena.2024.107947, 2024.

Baptista, J., Brito Guapo Teles Vieira, G., Manuel De Carvalho Soares Correia, A., Lee, H., and Westermann, S.: Modelling the evolution of permafrost temperatures and active layer thickness in King George Island, Antarctica, since 1950, The Cryosphere, 19, 3459–3476, https://doi.org/10.5194/tc-19-3459-2025, 2025.

Bi, D., Dix, M., Marsland, S., O'Farrell, S., Sullivan, A., Bodman, R., Law, R., Harman, I., Srbinovsky, J., Rashid, H. A., Dobrohotoff, P., Mackallah, C., Yan, H., Hirst, A., Savita, A., Dias, F. B., Woodhouse, M., Fiedler, R., and Heerdegen, A.: Configuration and spin-up of ACCESS-CM2, the new generation Australian Community Climate and Earth System Simulator Coupled Model, Journal of Southern Hemisphere Earth Systems Science, 70, 225–251, https://doi.org/10.1071/ES19040, 2020.

Birkenmajer, K.: A guide to Tertiary geochronology of King George Island, West Antarctica, 555–579, 1989.

Biskaborn, B. K., Smith, S. L., Noetzli, J., Matthes, H., Vieira, G., Streletskiy, D. A., Schoeneich, P., Romanovsky, V. E., Lewkowicz, A. G., Abramov, A., Allard, M., Boike, J., Cable, W. L., Christiansen, H. H., Delaloye, R., Diekmann, B., Drozdov, D., Etzelmüller, B., Grosse, G., Guglielmin, M., Ingeman-Nielsen, T., Isaksen, K., Ishikawa, M., Johansson, M., Johannsson, H., Joo, A., Kaverin, D., Kholodov, A., Konstantinov, P., Kröger, T., Lambiel, C., Lanckman, J.-P., Luo, D., Malkova, G., Meiklejohn, I., Moskalenko, N., Oliva, M., Phillips, M., Ramos, M., Sannel, A. B. K., Sergeev, D., Seybold, C., Skryabin, P., Vasiliev, A., Wu, Q., Yoshikawa, K., Zheleznyak, M., and Lantuit, H.: Permafrost is warming at a global scale, Nat Commun, 10, 264, https://doi.org/10.1038/s41467-018-08240-4, 2019.

Bockheim, J., Vieira, G., Ramos, M., López-Martínez, J., Serrano, E., Guglielmin, M., Wilhelm, K., and Nieuwendam, A.: Climate warming and permafrost dynamics in the Antarctic Peninsula region, Global and Planetary Change, 100, 215–223, https://doi.org/10.1016/j.gloplacha.2012.10.018, 2013.

Bonnet, R., Boucher, O., Deshayes, J., Gastineau, G., Hourdin, F., Mignot, J., Servonnat, J., and Swingedouw, D.: Presentation and Evaluation of the IPSL-CM6A-LR Ensemble of Extended Historical Simulations, J Adv Model Earth Syst, 13, e2021MS002565, https://doi.org/10.1029/2021MS002565, 2021.

Bozkurt, D., Bromwich, D. H., Carrasco, J., and Rondanelli, R.: Temperature and precipitation projections for the Antarctic Peninsula over the next two decades: contrasting global and regional climate model simulations, Clim Dyn, 56, 3853–3874, https://doi.org/10.1007/s00382-021-05667-2, 2021.

Bozkurt, D., Marín, J. C., and Barrett, B. S.: Temperature and moisture transport during atmospheric blocking patterns around the Antarctic Peninsula, Weather and Climate Extremes, 38, 100506, https://doi.org/10.1016/j.wace.2022.100506, 2022.

Bozkurt, D., Marín, J. C., Verdugo, C., and Barrett, B. S.: Atmospheric blocking and temperatures in the Antarctic Peninsula, Science of The Total Environment, 931, 172852, https://doi.org/10.1016/j.scitotenv.2024.172852, 2024.

https://doi.org/10.5194/egusphere-2026-1914
Preprint. Discussion started: 16 June 2026

Caillet, J., Jourdain, N. C., Mathiot, P., Gillet-Chaulet, F., Urruty, B., Burgard, C., Amory, C., Kittel, C., and Chekki, M.: Uncertainty in the projected Antarctic contribution to sea level due to internal climate variability, https://doi.org/10.5194/egusphere-2024-128, 8 February 2024.

Carrasco, J. F., Bozkurt, D., and Cordero, R. R.: A review of the observed air temperature in the Antarctic Peninsula. Did the warming trend come back after the early 21st hiatus?, Polar Science, 28, 100653, https://doi.org/10.1016/j.polar.2021.100653, 2021.

Copernicus Climate Change Service: CMIP6 predictions underpinning the C3S decadal prediction prototypes, https://doi.org/10.24381/CDS.C866074C, 2021.

Eyring, V., Bony, S., Meehl, G. A., Senior, C. A., Stevens, B., Stouffer, R. J., and Taylor, K. E.: Overview of the Coupled Model Intercomparison Project Phase 6 (CMIP6) experimental design and organization, Geosci. Model Dev., 9, 1937–1958, https://doi.org/10.5194/gmd-9-1937-2016, 2016.

Fernández-Fernández, J. M., Oliva, M., Palacios, D., Garcia-Oteyza, J., Navarro, F. J., Schimmelpfennig, I., Léanni, L., and Team, A.: Ice thinning on nunataks during the glacial to interglacial transition in the Antarctic Peninsula region according to Cosmic-Ray Exposure dating: Evidence and uncertainties, Quaternary Science Reviews, 264, 107029, https://doi.org/10.1016/j.quascirev.2021.107029, 2021.

Ferreira, A., Vieira, G., Ramos, M., and Nieuwendam, A.: Ground temperature and permafrost distribution in Hurd Peninsula (Livingston Island, Maritime Antarctic): An assessment using freezing indexes and TTOP modelling, CATENA, 149, 560–571, https://doi.org/10.1016/j.catena.2016.08.027, 2017.

Fox, A. J. (Ed.): Antarctic Peninsula: a visitor's guide, Second edition., Natural History Museum, London, 141 pp., 2019.

González-Herrero, S., Barriopedro, D., Trigo, R. M., López-Bustins, J. A., and Oliva, M.: Climate warming amplified the 2020 record-breaking heatwave in the Antarctic Peninsula, Commun Earth Environ, 3, 122, https://doi.org/10.1038/s43247-022-00450-5, 2022.

Gorodetskaya, I. V., Durán-Alarcón, C., González-Herrero, S., Clem, K. R., Zou, X., Rowe, P., Rodriguez Imazio, P., Campos, D., Leroy-Dos Santos, C., Dutrievoz, N., Wille, J. D., Chyhareva, A., Favier, V., Blanchet, J., Pohl, B., Cordero, R. R., Park, S.-J., Colwell, S., Lazzara, M. A., Carrasco, J., Gulisano, A. M., Krakovska, S., Ralph, F. M., Dethinne, T., and Picard, G.: Record-high Antarctic Peninsula temperatures and surface melt in February 2022: a compound event with an intense atmospheric river, npj Clim Atmos Sci, 6, 202, https://doi.org/10.1038/s41612-023-00529-6, 2023.

Gubler, S., Fiddes, J., Keller, M., and Gruber, S.: Scale-dependent measurement and analysis of ground surface temperature variability in alpine terrain, The Cryosphere, 5, 431–443, https://doi.org/10.5194/tc-5-431-2011, 2011.

Hersbach, H., Bell, B., Berrisford, P., Hirahara, S., Horányi, A., Muñoz-Sabater, J., Nicolas, J., Peubey, C., Radu, R., Schepers, D., Simmons, A., Soci, C., Abdalla, S., Abellan, X., Balsamo, G., Bechtold, P., Biavati, G., Bidlot, J., Bonavita, M., De Chiara, G., Dahlgren, P., Dee, D., Diamantakis, M., Dragani, R., Flemming, J., Forbes, R., Fuentes, M., Geer, A., Haimberger, L., Healy, S., Hogan, R. J., Hólm, E., Janisková, M., Keeley, S., Laloyaux, P., Lopez, P., Lupu, C., Radnoti, G., De Rosnay, P., Rozum, I., Vamborg, F., Villaume, S., and Thépaut, J.: The ERA5 global reanalysis, Quart J Royal Meteoro Soc, 146, 1999–2049, https://doi.org/10.1002/qj.3803, 2020.

Hrbáček, F., Oliva, M., Fernández, J.-R., Kňažková, M., and De Pablo, M. A.: Modelling ground thermal regime in bordering (dis)continuous permafrost environments, Environmental Research, 181, 108901, https://doi.org/10.1016/j.envres.2019.108901, 2020.

https://doi.org/10.5194/egusphere-2026-1914
Preprint. Discussion started: 16 June 2026

Hrbáček, F., Vieira, G., Oliva, M., Balks, M., Guglielmin, M., De Pablo, M. Á., Molina, A., Ramos, M., Goyanes, G., Meiklejohn, I., Abramov, A., Demidov, N., Fedorov-Davydov, D., Lupachev, A., Rivkina, E., Láska, K., Kňažková, M., Nývlt, D., Raffi, R., Strelin, J., Sone, T., Fukui, K., Dolgikh, A., Zazovskaya, E., Mergelov, N., Osokin, N., and Miamin, V.: Active layer monitoring in Antarctica: an overview of results from 2006 to 2015, Polar Geography, 44, 217–231, https://doi.org/10.1080/1088937X.2017.1420105, 2021.

Hrbáček, F., Oliva, M., Hansen, C., Balks, M., O'Neill, T. A., De Pablo, M. A., Ponti, S., Ramos, M., Vieira, G., Abramov, A., Kaplan Pastíriková, L., Guglielmin, M., Goyanes, G., Francelino, M. R., Schaefer, C., and Lacelle, D.: Active layer and permafrost thermal regimes in the ice-free areas of Antarctica, Earth-Science Reviews, 242, 104458, https://doi.org/10.1016/j.earscirev.2023.104458, 2023.

Hwang, J., Zheng, X., Ripley, E. M., Lee, J.-I., and Shin, D.: Isotope geochemistry of volcanic rocks from the Barton Peninsula, King George Island, Antarctica, J. Earth Sci., 22, 40–51, https://doi.org/10.1007/s12583-011-0156-y, 2011.

IPCC: Climate Change 2013: The Physical Science Basis. Contribution of Working Group I to the Fifth Assessment Report of the Intergovernmental Panel on Climate Change, 2013.

IPCC: Climate Change 2014: Synthesis Report. Contribution of Working Groups I, II and III to the Fifth Assessment Report of the Intergovernmental Panel on Climate Change [Core Writing Team, R.K. Pachauri and L.A. Meyer (eds.)], IPCC, 2014.

Jones, M. E., Bromwich, D. H., Nicolas, J. P., Carrasco, J., Plavcová, E., Zou, X., and Wang, S.-H.: Sixty Years of Widespread Warming in the Southern Middle and High Latitudes (1957–2016), Journal of Climate, 32, 6875–6898, https://doi.org/10.1175/JCLI-D-18-0565.1, 2019.

Jones, P. D. and Lister, D. H.: Antarctic near-surface air temperatures compared with ERA-Interim values since 1979, Int. J. Climatol., 35, 1354–1366, https://doi.org/10.1002/joc.4061, 2015.

Kim, H., Cho, M., and Lee, J.-I.: Thermal metamorphism of volcanic rocks on Barton Peninsula, King George Island, Antarctica, Geosci J, 6, 303–317, https://doi.org/10.1007/BF03020615, 2002.

Kiss, A. E., Hogg, A. McC., Hannah, N., Boeira Dias, F., Brassington, G. B., Chamberlain, M. A., Chapman, C., Dobrohotoff, P., Domingues, C. M., Duran, E. R., England, M. H., Fiedler, R., Griffies, S. M., Heerdegen, A., Heil, P., Holmes, R. M., Klocker, A., Marsland, S. J., Morrison, A. K., Munroe, J., Nikurashin, M., Oke, P. R., Pilo, G. S., Richet, O., Savita, A., Spence, P., Stewart, K. D., Ward, M. L., Wu, F., and Zhang, X.: ACCESS-OM2 v1.0: a global ocean–sea ice model at three resolutions, Geosci. Model Dev., 13, 401–442, https://doi.org/10.5194/gmd-13-401-2020, 2020.

Kraus, S., Miller, H., Dimov, D., Hegner, E., McWilliams, M., and Pecskay, Z.: Structural geology of the Mesozoic Miers Bluff Formation and crosscutting Paleogene dikes (Livingston Island, South Shetland Islands, Antarctica) – Insights into the geodynamic history of the northern Antarctic Peninsula, Journal of South American Earth Sciences, 26, 498–512, https://doi.org/10.1016/j.jsames.2008.08.009, 2008.

Lopez-Martinez, J., Pison, M. de, and Arche, A.: Geomorphology of Hurd Península, Livingston Island, South Shetland Islands, Progress in Antarctic Earth Science, 751–756, 1992.

López-Martínez, J., Serrano, E., Schmid, T., Mink, S., and Linés, C.: Periglacial processes and landforms in the South Shetland Islands (northern Antarctic Peninsula region), Geomorphology, 155–156, 62–79, https://doi.org/10.1016/j.geomorph.2011.12.018, 2012.

https://doi.org/10.5194/egusphere-2026-1914
Preprint. Discussion started: 16 June 2026

Mathiot, P., Jenkins, A., Harris, C., and Madec, G.: Explicit representation and parametrised impacts of under ice shelf seas in the z^* coordinate ocean model NEMO 3.6, Geosci. Model Dev., 10, 2849–2874, https://doi.org/10.5194/gmd-10-2849-2017, 2017.

Matsuoka, K., Skoglund, A., Roth, G., de Pomereu, J., Griffiths, H., Headland, R., Herried, B., Katsumata, K., Le Brocq, A., Licht, K., Morgan, F., Neff, P., Ritz, C., Scheinert, M., Tamura, T., Van de Putte, A., van den Broeke, M., von Deschwanden, A., Deschamps-Berger, C., Van Liefferinge, B., Tronstad, S., Melvær, Y., Norwegian Polar Institute, Matsuoka, K., Skoglund, A., and Roth, G.: Quantarctica, https://doi.org/10.21334/NPOLAR.2018.8516E961, 2018.

Morioka, Y., Zhang, L., Cooke, W., Nonaka, M., Behera, S. K., and Manabe, S.: Role of anthropogenic forcing in Antarctic sea ice variability simulated in climate models, Nat Commun, 15, 10511, https://doi.org/10.1038/s41467-024-54485-7, 2024.

Obu, J., Westermann, S., Vieira, G., Abramov, A., Balks, M., Bartsch, A., Hrbáček, F., Kääb, A., and Ramos, M.: Pan-Antarctic map of near-surface permafrost temperatures at 1 km^2 scale, The Cryosphere, https://doi.org/10.5194/tc-2019-148, 2020.

Oliva, M., Navarro, F., Hrbáček, F., Hernández, A., Nývlt, D., Pereira, P., Ruiz-Fernández, J., and Trigo, R.: Recent regional climate cooling on the Antarctic Peninsula and associated impacts on the cryosphere, Science of The Total Environment, 580, 210–223, https://doi.org/10.1016/j.scitotenv.2016.12.030, 2017.

Oliva, M., Antoniades, D., Serrano, E., Giralt, S., Liu, E. J., Granados, I., Pla-Rabes, S., Toro, M., Hong, S. G., and Vieira, G.: The deglaciation of Barton Peninsula (King George Island, South Shetland Islands, Antarctica) based on geomorphological evidence and lacustrine records, Polar Record, 55, 177–188, https://doi.org/10.1017/S0032247419000469, 2019.

Oliva, M., Palacios, D., Sancho, L. G., Fernández-Fernández, J. M., Çiner, A., Fernandes, M., García-Oteyza, J., Sarıkaya, M. A., Serrano, E., Kaveh-Firouz, A., Pérez-Alberti, A., Schimmelpfennig, I., Vieira, G., Bonsoms, J., and Antoniades, D.: The origin of the ice-free areas of the Hurd Peninsula (Livingston Island, Antarctica), Quaternary Science Reviews, 344, 108991, https://doi.org/10.1016/j.quascirev.2024.108991, 2024.

O'Neill, B. C., Tebaldi, C., Van Vuuren, D. P., Eyring, V., Friedlingstein, P., Hurtt, G., Knutti, R., Kriegler, E., Lamarque, J.-F., Lowe, J., Meehl, G. A., Moss, R., Riahi, K., and Sanderson, B. M.: The Scenario Model Intercomparison Project (ScenarioMIP) for CMIP6, Geosci. Model Dev., 9, 3461–3482, https://doi.org/10.5194/gmd-9-3461-2016, 2016.

Rashid, H. A., Sullivan, A., Dix, M., Bi, D., Mackallah, C., Ziehn, T., Dobrohotoff, P., O'Farrell, S., Harman, I. N., Bodman, R., and Marsland, S.: Evaluation of climate variability and change in ACCESS historical simulations for CMIP6, Journal of Southern Hemisphere Earth Systems Science, 72, 73–92, https://doi.org/10.1071/ES21028, 2022.

Schroeter, S., Bi, D., Law, R. M., Loughran, T. F., Rashid, H. A., and Wang, Z.: Global-scale future climate projections from ACCESS model contributions to CMIP6, Journal of Southern Hemisphere Earth Systems Science, 74, ES23029, https://doi.org/10.1071/ES23029, 2024.

Sun, Y., Zhang, Y., Wang, Y., Heil, P., Hou, S., and Zhai, Z.: Constraining Future Antarctic Warming Under Five Different Emissions Scenarios in the CMIP6 Multi-Models, Geophysical Research Letters, 52, e2024GL112662, https://doi.org/10.1029/2024GL112662, 2025.

Tetzner, D., Thomas, E., and Allen, C.: A Validation of ERA5 Reanalysis Data in the Southern Antarctic Peninsula—Ellsworth Land Region, and Its Implications for Ice Core Studies, Geosciences, 9, 289, https://doi.org/10.3390/geosciences9070289, 2019.

https://doi.org/10.5194/egusphere-2026-1914
Preprint. Discussion started: 16 June 2026

Tewari, K., Mishra, S. K., Salunke, P., and Dewan, A.: Future projections of temperature and precipitation for Antarctica, Environ. Res. Lett., 17, 014029, https://doi.org/10.1088/1748-9326/ac43e2, 2022.

Thomas, E. and Tetzner, D.: The Climate of the Antarctic Peninsula during the Twentieth Century: Evidence from Ice Cores, in: Antarctica - A Key To Global Change, edited by: Kanao, M., Toyokuni, G., and Yamamoto, M., IntechOpen, https://doi.org/10.5772/intechopen.81507, 2019.

Turner, J., Phillips, T., Hosking, J. S., Marshall, G. J., and Orr, A.: The Amundsen Sea low, Intl Journal of Climatology, 33, 1818–1829, https://doi.org/10.1002/joc.3558, 2013.

Turner, J., Marshall, G. J., Clem, K., Colwell, S., Phillips, T., and Lu, H.: Antarctic temperature variability and change from station data, Intl Journal of Climatology, 40, 2986–3007, https://doi.org/10.1002/joc.6378, 2020.

Vaughan, D. G., Marshall, G. J., Connolley, W. M., Parkinson, C., Mulvaney, R., Hodgson, D. A., King, J. C., Pudsey, C. J., and Turner, J.: Recent Rapid Regional Climate Warming on the Antarctic Peninsula, Climatic Change, 60, 243–274, https://doi.org/10.1023/A:1026021217991, 2003.

Vieira, G., Bockheim, J., Guglielmin, M., Balks, M., Abramov, A. A., Boelhouwers, J., Cannone, N., Ganzert, L., Gilichinsky, D. A., Goryachkin, S., López-Martínez, J., Meiklejohn, I., Raffi, R., Ramos, M., Schaefer, C., Serrano, E., Simas, F., Sletten, R., and Wagner, D.: Thermal state of permafrost and active-layer monitoring in the antarctic: Advances during the international polar year 2007–2009, Permafrost & Periglacial, 21, 182–197, https://doi.org/10.1002/ppp.685, 2010.

Vionnet, V., Brun, E., Morin, S., Boone, A., Faroux, S., Le Moigne, P., Martin, E., and Willemet, J.-M.: The detailed snowpack scheme Crocus and its implementation in SURFEX v7.2, Geosci. Model Dev., 5, 773–791, https://doi.org/10.5194/gmd-5-773-2012, 2012.

Volodin, E., Mortikov, E., Gritsun, A., Lykossov, V., Galin, V., Diansky, N., Gusev, A., Kostrykin, S., Iakovlev, N., Shestakova, A., and Emelina, S.: INM INM-CM4-8 model output prepared for CMIP6 CMIP historical (20250528), https://doi.org/10.22033/ESGF/CMIP6.5069, 2019.

Westermann, S., Langer, M., Boike, J., Heikenfeld, M., Peter, M., Etzelmüller, B., and Krinner, G.: Simulating the thermal regime and thaw processes of ice-rich permafrost ground with the land-surface model CryoGrid 3, Geosci. Model Dev., 9, 523–546, https://doi.org/10.5194/gmd-9-523-2016, 2016.

Westermann, S., Ingeman-Nielsen, T., Scheer, J., Aalstad, K., Aga, J., Chaudhary, N., Etzelmüller, B., Filhol, S., Kääb, A., Renette, C., Schmidt, L. S., Schuler, T. V., Zweigel, R. B., Martin, L., Morard, S., Ben-Asher, M., Angelopoulos, M., Boike, J., Groenke, B., Miesner, F., Nitzbon, J., Overduin, P., Stuenzi, S. M., and Langer, M.: The CryoGrid community model (version 1.0) – a multi-physics toolbox for climate-driven simulations in the terrestrial cryosphere, Geoscientific Model Development, 16, 2607–2647, https://doi.org/10.5194/gmd-16-2607-2023, 2023.

Wilhelm, K. and Bockheim, J.: Influence of soil properties on active layer thermal propagation along the western Antarctic Peninsula, Earth Surf Processes Landf, 41, 1550–1563, https://doi.org/10.1002/esp.3926, 2016.

Wilhelm, K. R. and Bockheim, J. G.: Climatic controls on active layer dynamics: Amsler Island, Antarctica, Antarctic Science, 29, 173–182, https://doi.org/10.1017/S0954102016000511, 2017.

Wilhelm, K. R., Bockheim, J. G., and Haus, N. W.: Properties and processes of recently established soils from deglaciation of Cierva Point, Western Antarctic Peninsula, Geoderma, 277, 10–22, https://doi.org/10.1016/j.geoderma.2016.05.001, 2016.

https://doi.org/10.5194/egusphere-2026-1914
Preprint. Discussion started: 16 June 2026

Zhu, J., Xie, A., Qin, X., Wang, Y., Xu, B., and Wang, Y.: An Assessment of ERA5 Reanalysis for Antarctic Near-Surface Air Temperature, Atmosphere, 12, 217, https://doi.org/10.3390/atmos12020217, 2021.

Zhu, J., Xie, A., Wang, S., Qin, X., Li, B., Xu, B., and Wang, Y.: Future Antarctic amplification from extreme temperature indices for different socioeconomic scenarios and time periods, J. South. Hemisph. Earth Syst. Sci., 75, https://doi.org/10.1071/ES24009, 2025.

Zou, X., Rowe, P. M., Gorodetskaya, I., Bromwich, D. H., Lazzara, M. A., Cordero, R. R., Zhang, Z., Kawzenuk, B., Cordeira, J. M., Wille, J. D., Ralph, F. M., and Bai, L.: Strong Warming Over the Antarctic Peninsula During Combined Atmospheric River and Foehn Events: Contribution of Shortwave Radiation and Turbulence, JGR Atmospheres, 128, e2022JD038138, https://doi.org/10.1029/2022JD038138, 2023.

Zweigel, R. B., Westermann, S., Nitzbon, J., Langer, M., Boike, J., Etzelmüller, B., and Vikhamar Schuler, T.: Simulating Snow Redistribution and its Effect on Ground Surface Temperature at a High-Arctic Site on Svalbard, JGR Earth Surface, 126, e2020JF005673, https://doi.org/10.1029/2020JF005673, 2021.